Agricultural and Forest Meteorology 214-215 (2015) 515–531

Contents lists available at ScienceDirect

Agricultural and Forest Meteorology

journal homepage: www.elsevier.com/locate/agrformet

An improved isotopic method for partitioning net ecosystem–atmosphere CO_2 exchange

R. Wehr*, S.R. Saleska

Department of Ecology and Evolutionary Biology, University of Arizona, 1041 E. Lowell St., Tucson, AZ 85721, USA

ARTICLE INFO

Article history:
Received 17 April 2015
Received in revised form
11 September 2015
Accepted 17 September 2015

Keywords:
Carbon dioxide
Net ecosystem exchange
Partitioning
Eddy covariance
Isotope
Forest

ABSTRACT

Stable carbon isotopes can be used to partition the net ecosystem–atmosphere exchange (NEE) of carbon dioxide (CO_2) into its photosynthetic and respiratory components, but the method has not been generally adopted due to instrumental and theoretical limitations. Here, motivated by recently improved instrumentation, we extend the theory of isotopic flux partitioning to include photorespiration, foliar daytime 'dark' respiration, and other refinements, arriving at a general yet practical formulation from which all previous formulations can be derived as simplifying approximations. We use a full growing season of isotopic eddy covariance flux data from a temperate deciduous forest to demonstrate the method, quantify its uncertainties, and determine biases associated with previously published formulations. We find that when $\delta^{13}C$ of CO_2 is acquired with high precision (0.02‰ RMSE for 100 s integration times), the statistical uncertainty in the partitioned fluxes is comparable to that in NEE itself—i.e., as good as practicably possible. Assessable systematic uncertainty is ±17% of gross ecosystem production (GEP), due mostly to uncertainty in the isotopic fractionation by carboxylation. Additional, currently unquantifiable systematic uncertainty is associated with treating the canopy as a single "big leaf". Both sources of systematic uncertainty could be greatly reduced by feasible supporting leaf-level measurements. Our extended theory corrects systematic biases in previous isotopic approaches, including overestimation (by 13%) of GEP due to the omission of photorespiration. The partitioning determines the isotopic signature of photosynthesis, which we find to vary seasonally between −24 and −28‰ such that the isotopic disequilibrium between ecosystem carbon input and output remains stable at approximately −0.5‰ through most of the growing season. The key advantage of isotopic partitioning over standard, regression-based partitioning is that it enables controls on the ecosystem-scale photosynthetic and respiratory fluxes to emerge from observations, without having to assume functional relations to environmental drivers *a priori*. As an example, we show how isotopic partitioning reveals certain large variations in daytime NEE to be caused by shifts in the flux tower sampling footprint between regions of high and low respiratory flux—a finding unobtainable by standard partitioning. For this reason, isotopic partitioning can be more precise than standard partitioning for quantifying environmental controls on NEE.

1. Introduction

The net ecosystem–atmosphere exchange of CO_2 (NEE) is routinely measured by eddy covariance at hundreds of tower sites around the world (Baldocchi, 2008; Luyssaert et al., 2009). NEE is the balance of ecosystem photosynthesis and ecosystem respiration, and most analyses of NEE involve partitioning it into these somewhat independent and somewhat coupled components. There being no means to measure each component directly, standard empirical flux partitioning (Lasslop et al., 2010; Reichstein et al., 2005; Stoy et al., 2006) works by prescribing the functional forms of the responses of ecosystem-scale photosynthesis and/or respiration to environmental drivers based on inferences drawn from leaf or soil-plot gas exchange measurements or from nighttime NEE. Isotopic flux partitioning (IFP) is an alternative that avoids such assumptions, instead identifying the photosynthetic and respiratory components of NEE by their distinct stable isotopic signatures—here ^{13}C *versus* ^{12}C. The ratio of ^{13}C to ^{12}C differs between photosynthesized and respired carbon chiefly because there is a strong isotopic fractionation by photosynthesis that varies on timescales shorter than the mean age of the substrate for respiration. Isotopic partitioning has not seen general use because of

* Corresponding author at: Department of Earth and Planetary Sciences, Harvard University, 24 Oxford St., Cambridge, MA 02138, USA.
E-mail addresses: rawehr@email.arizona.edu (R. Wehr), saleska@email.arizona.edu (S.R. Saleska).

http://dx.doi.org/10.1016/j.agrformet.2015.09.009
0168-1923/

limits on both the precision of *in situ* isotope measurements and the theory used to apply those measurements to the partitioning problem.

That theory has been developed through a succession of studies (Billmark and Griffis, 2009; Bowling et al., 2001; Fassbinder et al., 2012; Knohl and Buchmann, 2005; Lai et al., 2003; Ogée et al., 2003; Yakir and Wang, 1996; Zhang et al., 2006; Zobitz et al., 2008), as recently reviewed by Fassbinder et al. (2012). Motivated by recently developed spectroscopic technology for high-precision ^{13}C measurements in atmospheric CO_2 (Wehr et al., 2013), we elaborate the theory further, incorporating photorespiration, foliar daytime 'dark' respiration, and several other refinements to arrive at a general but practical formulation (Section 2) from which all previously published formulations can be derived as approximations. We then use a full growing season of isotopic eddy covariance measurements (Wehr et al., 2013) and supporting data from a temperate forest (Section 3) to demonstrate the partitioning, to quantify its uncertainties, and to quantify biases associated with previous formulations (Section 4). Appendix A provides some fundamental definitions; Appendix B provides a detailed accounting of the resistances, fractionations, and other input parameters we selected for our oak-dominated forest ecosystem; and Appendix C summarizes the differences between the present formulation and those previously published.

2. Isotopic flux partitioning equations

The basic idea of isotopic flux partitioning (Bowling et al., 2001; Ogée et al., 2003; Yakir and Wang, 1996) is to determine the magnitudes of the photosynthetic and respiratory gross fluxes using their isotopic signatures and the isotopic composition and magnitude of their sum (i.e. NEE); that is, to solve the set of two equations describing the isotopic mass balance of CO_2 in the forest,

$$F_N = F_A + F_{NR} \tag{1}$$

$$\delta_N F_N = \delta_A F_A + \delta_{NR} F_{NR}, \tag{2}$$

for the unknowns F_A and F_{NR}, where the ecosystem-scale fluxes F and their isotopic compositions δ are labeled by the following subscripts: N for NEE, A for canopy net photosynthetic assimilation, and NR for non-foliar ecosystem respiration. In this article, δ is shorthand for $\delta^{13}C$, which is the ratio of ^{13}C to ^{12}C expressed as a relative difference from a standard material (see Appendix A).

Solving this pair of equations requires knowledge of the isotopic composition of NEE (δ_N), the isotopic signature of non-foliar ecosystem respiration (δ_{NR}), and the isotopic signature of net photosynthetic assimilation (δ_A). δ_N can be measured directly, and δ_{NR} can be obtained from a combination of soil chamber and nighttime Keeling plot measurements as detailed in Section 3.2. δ_A, however, cannot be measured at the ecosystem scale with the required time resolution. Instead, the approach generally taken is to use our understanding of photosynthetic fractionation (also called discrimination) by individual leaves to express δ_A in terms of F_A, so that δ_A can be eliminated from the above equations (and thus solved for as part of the partitioning). In the original formulation of this approach (Bowling et al., 2001), the link between δ_A and F_A consisted simply of Fick's law for CO_2 diffusion through the leaf stomata,

$$F_A = -g_s(c_a - c_i), \tag{3}$$

and the well-known simplified equation for photosynthetic fractionation (Farquhar et al., 1982),

$$\varepsilon_A = \varepsilon_s + (b - \varepsilon_s)\frac{c_i}{c_a}, \tag{4}$$

along with an approximate definition of the photosynthetic fractionation,

$$\varepsilon_A \approx \delta_a - \delta_A \tag{5}$$

(cf. the exact definition in Appendix A). In the above equations, g_s is the stomatal conductance, c_i is the intercellular CO_2 concentration inside the leaf, c_a and δ_a are the CO_2 concentration and isotopic composition of the air outside the leaf, ε_A is the apparent isotopic fractionation of canopy net photosynthetic assimilation (often written as Δ), ε_s is the fractionation associated with diffusion of CO_2 through the stomata (4.4‰), and b is the apparent fractionation associated with fixation of intercellular CO_2 (~27‰). Combining these equations eliminates c_i and ε_A and gives δ_A in terms of F_A—provided that atmospheric CO_2 is measured, that stomatal conductance can be determined (e.g. from measured ecosystem-scale heat and water fluxes), and that ε_s and b are known constants. The above fractionation equation, Eq. (4), neatly expresses the central fact that the fractionation by photosynthesis depends on the relative rates of CO_2 diffusion and fixation, being weighted toward the fractionation associated with whichever of those two processes is most limiting to the overall rate of assimilation (because diffusion limitation will cause c_i to approach zero while fixation limitation will cause c_i to approach c_a).

This basic approach for estimating the canopy-scale isotopic signature of photosynthesis (and the more comprehensive one we develop here below) relies on the assumption that our understanding of leaf-level photosynthetic fractionation (Farquhar et al., 1982) can be scaled directly to the canopy. This approach, in which the whole canopy is treated as a single "big leaf", requires that the response of the distribution of leaves in the canopy to the distribution of environmental conditions that they experience can be approximated by the response of a single "big leaf" to the average environmental conditions. Such an approximation is insufficient for some analyses (De Pury and Farquhar, 1997), but big leaf approaches have nonetheless been shown to accurately capture key aspects of canopy photosynthesis (Amthor et al., 1994; Lloyd et al., 1995), and in this case, there are insufficient observational data at present to constrain a more complex dual- or multi-leaf model. Note, however, that carbon isotope discrimination has been considered in a multi-leaf framework before (Baldocchi and Bowling, 2003; Ogée et al., 2003).

Note also that we depart from some of the notation inherited through the lineage of IFP studies, sacrificing continuity in favor of a standardized notation consistent with guidelines in Coplen (2011) (wherein, e.g., ε represents isotopic fractionation, leading us to use ε_A rather than Δ for photosynthetic fractionation). Our symbols and notations are explained in Tables 1 and 2, and several key variables are defined in Appendix A. Except in a few special cases, each property (e.g. fractionation) is given a unique letter or symbol (e.g. ε), and the property is associated with specific sites (e.g. above the canopy) or processes (e.g. dissolution) by subscripts. Superscripts 12 and 13 specify the carbon isotopes.

2.1. Carbon isotope mass balance

We begin by expanding the terms of the mass balance of CO_2 in the forest air (Eq. (1)) to now explicitly include the photorespiration flux F_{PR}, the foliar daytime 'dark' respiration flux F_{DR}, and the non-foliar (mostly belowground) respiration flux F_{NR}:

$$F_N = F_P + F_{PR} + F_{DR} + F_{NR}. \tag{6}$$

All the fluxes F are at the ecosystem scale and are positive when directed into the atmosphere. We define gross ecosystem production by GEP $\equiv -(F_P + F_{PR})$, ecosystem respiration by $R_{eco} \equiv F_{DR} + F_{NR}$, and the canopy net CO_2 assimilation flux by $F_A \equiv F_P + F_{PR} + F_{DR}$.

Table 1
Key to symbols.

Symbol	Description	Units
F	Flux (formally flux density) of CO_2	mol m^{-2} s^{-1}
H	Flux (formally flux density) of sensible heat	W m^{-2}
E	Flux (formally flux density) of water vapor	mol m^{-2} s^{-1}
R	Isotope atom ratio, $^{13}C/^{12}C$	–
δ	Relative difference of R from R_{VPDB}	–
α	Isotopic fractionation factor	–
ε	Isotopic fractionation ($=\alpha-1$)	–
c	Concentration of CO_2	mol m^{-3}
C	Mole fraction of CO_2 in air	mol mol^{-1}
C_p	Specific heat capacity of air	J kg^{-1} K^{-1}
r	Resistance	s m^{-1}
g	Conductance ($=1/r$)	m s^{-1}
e	Vapor pressure	Pa
T	Temperature	K
P	Air pressure	Pa
ρ	Density of air	kg m^{-3}
γ	Psychrometric constant	Pa K^{-1}
λ	Latent heat of vaporization of water	J mol^{-1}
k_H	Henry's constant ($=c_{ow}/c_i$)	–
a	Flux measurement height	m
h	Canopy top height	m
Sc	Schmidt number for CO_2	–
Sc_V	Schmidt number for water vapor	–
Pr	Prandtl number for air	–
Γ'_*	Photocompensation point	mol mol^{-1}
u	Wind speed	m s^{-1}
u_*	Friction velocity	m s^{-1}
χ	Clear sky index	–
β	Fraction of carboxylation performed by PEP-carboxylase	–

Table 2
Key to subscripts.

Subscript	Meaning
Processes	
N	Net ecosystem–atmosphere CO_2 exchange (NEE)
P	Gross photosynthesis (uptake is negative)
PR	Photorespiration
DR	Foliar daytime 'dark' respiration
A	Net foliar photosynthetic assimilation
NR	Non-foliar (heterotroph, root, and stem) respiration
e	Turbulent eddy 'diffusion'
b	Leaf boundary layer diffusion of CO_2
bH	Leaf boundary layer diffusion of heat
bV	Leaf boundary layer diffusion of water vapor
s	Stomatal diffusion of CO_2
sV	Stomatal diffusion of water vapor
d	Dissolution of CO_2 in water
hyd	Hydration of CO_2
m	Mesophyll diffusion of CO_2
wp	Mesophyll cell wall and plasmalemma diffusion of CO_2
ch	Chloroplast envelope and stroma diffusion of CO_2
f	Enzyme-catalyzed fixation of CO_2
Ru	Carboxylation by Rubisco
Locations	
a	Above the canopy, at flux measurement height
h	Top of canopy
n	Within the canopy
u	Under the leaf boundary layer, outside the stomata
i	In the leaf intercellular airspace
ow	In the liquid lining the outside of the mesophyll cell walls
c	At the site of carboxylation
L	Throughout the leaf

Eq. (6) applies to total CO_2 and to $^{12}CO_2$ and $^{13}CO_2$ individually, so that twice applying it leads to:

$$R_N F_N = R_P F_P + R_{PR} F_{PR} + R_{DR} F_{DR} + R_{NR}(F_N - F_P - F_{PR} - F_{DR}), \quad (7)$$

where the R are absolute ratios of ^{13}C to ^{12}C. Eq. (7) is exact if the fluxes refer to ^{12}C, and is a good approximation if they refer to total carbon, i.e. as written (Tans et al., 1993). Because the proportional differences between the isotopic ratios R_N, R_P, R_{PR}, R_{DR}, and R_{NR} are less than about 10‰, the maximum proportional error in any term in Eq. (7) when all the ^{12}C fluxes are replaced with total C fluxes is less than about 0.1‰.

There are 9 variables in Eq. (7), only 3 of which (R_N, F_N, R_{NR}) are measured here. To solve for the remaining variables, we require five additional equations in F_P, R_P, F_{PR}, R_{PR}, F_{DR}, and R_{DR}, the derivation of which is the subject of Sections 2.2 and 2.3.

2.2. Photorespiration and foliar daytime 'dark' respiration

We have no means to measure F_P, F_{PR}, and F_{DR} independently, and because photorespiration (F_{PR}) and foliar daytime 'dark' respiration (F_{DR}) fractionate the carbon isotopes (i.e. $R_P \neq R_{PR} \neq R_{DR}$) (Ghashghaie et al., 2003; Igamberdiev et al., 2004; Lanigan et al., 2008; Tcherkez, 2006; Tcherkez et al., 2004, 2010), we cannot simply wrap them into net assimilation and ignore them. Fortunately, the published literature provides a useful empirical understanding of photorespiration and foliar daytime 'dark' respiration.

Photorespiration is the dominant component of daytime foliar CO_2 production, with photorespiratory carbon loss equal to about one fifth the net photosynthetic carbon gain in C_3 plants (Bauwe et al., 2010). The photorespiratory flux is known to depend on the available light, the temperature, and the O_2 and CO_2 concentrations at the site of carboxylation (Sharkey, 1988). In particular, Eqs. (4), (5a) and (8) of Sharkey (1988) can be used to write:

$$F_{PR} = -F_P \Gamma'_* / C_c, \quad (8)$$

where $C_c = (c_c/k_H)/c_{air}$ is the gas-phase equivalent molar mixing ratio of chloroplast CO_2 to (wet) air and Γ'_* is the photocompensation point expressed as a gas-phase equivalent molar mixing ratio of CO_2 to (wet) air. Here c_c is the concentration of CO_2 at the site of carboxylation in the chloroplast, k_H is Henry's constant, and c_{air} is the moles of (wet) air per unit volume in the forest canopy. An expression for c_c/k_H is derived in Section 2.3, and an empirical formula for Γ'_* as a function of temperature under ambient O_2 is provided in Appendix B6. The measured temperature and pressure at flux measurement height can be used to calculate a sufficiently accurate c_{air} via the ideal gas law.

The carbon isotope fractionation by photorespiration has been considered in detail by Tcherkez (2006), whose Eq. (B2) is, in our notation:

$$R_{PR} = \frac{a_0}{1 + a_1(F_{PR}/F_P)} R_P, \quad (9)$$

where

$$a_0 = \frac{2(1+\varepsilon)}{(2+g)}; \quad a_1 = \frac{2(1+\varepsilon)(1+g)}{(2+g)} - 1 \quad (10)$$

and where, in turn, $\varepsilon \sim 1$‰ is a parameter (not strictly a fractionation, unlike elsewhere in this article) that depends on the fractionation by aldolase and transketolase, and $g \sim 22$‰ is the fractionation by glycine decarboxylase (Tcherkez, 2006). These values are discussed in Appendix B8.

Having established equations for the flux and isotopic composition of photorespiration, we turn to foliar daytime 'dark' respiration, which has not been well described by measurement or theory. At this point, even the substrate is uncertain; however Tcherkez et al. (2010) have reported that the substrate for foliar 'dark' respiration in the light is similar to that in the dark—though the metabolic pathway (and hence fractionation) differs—and Nogués et al. (2004) have reported that the substrate for foliar 'dark' respiration after the cessation of illumination is not composed of recent photosynthates. Nonetheless, the isotopic fractionation by daytime 'dark' respiration is generally defined by assuming that the substrate has the same isotopic composition as

recent net assimilates—that, for example, is the way in which the fractionation parameter e is defined in the full discrimination equation of Farquhar et al. (1982). Based on that assumption, foliar 'dark' respiration in the dark is thought to discriminate against ^{12}C (by up to 6‰), while foliar 'dark' respiration in the light is thought to discriminate against ^{13}C (by about 5‰) (Tcherkez et al., 2004, 2010).

Fortunately for IFP, foliar daytime 'dark' respiration should be much smaller than photorespiration, and is inhibited by sunlight in some species (Hurry et al., 2005; Pärnik and Keerberg, 2007)—though it is unknown whether such inhibition occurs in the oak leaves considered here. Xu and Griffin (2008) estimated mean nightly foliar respiration for the period from June to October in dry and mesic red oak stands in New York State (from a model) and reported 45 mmol m^{-2} $night^{-1}$ for the dry stand and 101 mmol m^{-2} $night^{-1}$ for the mesic stand, which correspond to about 1.5 μmol m^{-2} s^{-1} and 3.5 μmol m^{-2} s^{-1}, respectively. Given our June-to-October mean nighttime NEE of 5.2 μmol m^{-2} s^{-1}, Xu and Griffin (2008)'s findings would suggest that foliar respiration accounts for one quarter to one half of our nighttime NEE. For the partitioning presented in this article, we simply assume that foliar daytime 'dark' respiration is one quarter of nighttime R_{eco}. Thus F_{DR} is calculated as:

$$F_{DR} = 0.25R^*_{eco}, \tag{11}$$

where R^*_{eco} is R_{eco} for the same wind direction as F_{DR}, obtained from a whole-season Loess-smoothing of nighttime NEE *versus* wind direction.

We also make the usual assumption that the substrate for daytime 'dark' respiration has the same isotopic composition as recent net photosynthates, in which case,

$$R_{DR} = \frac{R_A}{\alpha_{DR}} = \frac{\left(\frac{R_P F_P + R_{PR} F_{PR} + R_{DR} F_{DR}}{F_P + F_{PR} + F_{DR}}\right)}{\alpha_{DR}}, \tag{12}$$

where α_{DR} is the fractionation factor for daytime 'dark' respiration (see Appendix B8), and where in the expansion of R_A, we have replaced ^{12}C fluxes by total C fluxes as in Eq. (7). Rearranging Eq. (12) to isolate R_{DR}, and then inserting Eq. (9) to eliminate R_{PR}, yields:

$$R_{DR} = \frac{F_P + \frac{a_0}{1+a_1(F_{PR}/F_P)} F_{PR}}{\alpha_{DR}(F_P + F_{PR} + F_{DR}) - F_{DR}} R_P. \tag{13}$$

The errors resulting from the assumed substrate composition and rate for daytime 'dark' respiration should be small given the low sensitivity of IFP to F_{DR} and R_{DR} (Section 4.4).

2.3. CO_2 transport and fixation within the leaf

Two tasks remain: (1) deriving the final equation, which must relate the gross photosynthetic flux F_P to its isotopic composition R_P, and (2) deriving an expression for c_c/k_H to insert into Eq. (8). Both tasks require us to consider the series of diffusive and biochemical processes by which leaves assimilate atmospheric CO_2. We depict those processes in Fig. 1, adapted from Tholen et al. (2012). To reach the site of carboxylation (subscript c) in the chloroplast, CO_2 from the canopy air (n) must diffuse through: the leaf boundary layer (b), the stomata (s), the mesophyll cell wall and plasmalemma (wp), and the chloroplast envelope and stroma (ch). Along the way, CO_2 passing from the intercellular air space to the cell wall must dissolve in water according to Henry's constant k_H. Simultaneously, photorespiration and foliar daytime 'dark' respiration are producing CO_2, which is injected into the cytosol (y) by the mitochondria, partway along the transport pathway. Each of these processes has its own isotope-specific rate constant.

Approximating the CO_2 transport as one-dimensional, Fick's Law (Eq. (A1)) defines a resistance r to the diffusion of each isotope through each component of the leaf. We follow Tholen et al.

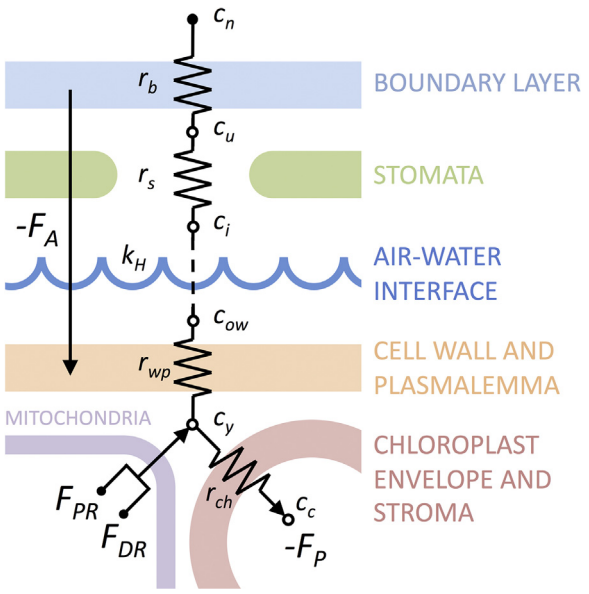

Fig. 1. Schematic diagram of CO_2 production, consumption, and transport in and around the leaf. The various r are resistances to CO_2 transport, the various c are CO_2 concentrations, and the various F are CO_2 fluxes. Subscripts are explained in Table 2. *Source*: Adapted from Tholen et al. (2012).

(2012) in assuming that the resistances of the intercellular air space (i) and the cytosol (y) are much less than those of the cell wall, plasmalemma, chloroplast envelope, and stroma (an uncertain but necessary assumption given the present state of knowledge: see Evans and Caemmerer, 1996; Flexas et al., 2008; Gillon and Yakir, 2000; Mott and O'Leary, 1984; Parkhurst and Mott, 1990). Thus the total mesophyll resistance is $r_m \approx r_{wp} + r_{ch}$, and we can write the following equations for diffusion against the component resistances r_{wp} and r_{ch}:

$$c_y - c_c = -r_{ch} F_P \tag{14}$$

$$c_{ow} - c_y = -r_{wp} F_A = -r_{wp}(F_P + F_{PR} + F_{DR}), \tag{15}$$

where c_{ow} is the concentration just outside the cell wall, in solution. This concentration is related to c_i by Henry's Law:

$$c_{ow} = k_H c_i, \tag{16}$$

where Henry's constant k_H is about 0.8 but is different for each isotope. Eq. (16) assumes that exchange of CO_2 across the gas–liquid interface is very much faster than diffusion of CO_2 in air or water (a good assumption according to Siegenthaler and Munnich, 1981).

Similarly, for the gas-phase diffusion path, we can write:

$$c_n - c_i = -(r_b + r_s) F_A = -(r_b + r_s)(F_P + F_{PR} + F_{DR}). \tag{17}$$

Eqs. (14)–(17) can be combined to yield:

$$\frac{c_c}{k_H} = c_n + (r_b + r_s + x_{wp} + x_{ch}) F_P + (r_b + r_s + x_{wp})(F_{PR} + F_{DR}), \tag{18}$$

where we have introduced the gas-phase equivalent resistance $x = r/k_H$. At this point it is useful to introduce the abbreviations,

$$r_1 = r_b + r_s + x_{wp} + x_{ch} \tag{19}$$

$$r_2 = r_b + r_s + x_{wp}, \tag{20}$$

and to use Eq. (A3) to define $\alpha_1 \equiv r_1^{13}/r_1^{12}$ and $\alpha_2 \equiv r_2^{13}/r_2^{12}$. Because Eqs. (14)–(20) apply separately to each isotope as well as to total CO_2, we have:

$$\alpha_1 = \frac{\alpha_b r_b^{12} + \alpha_s r_s^{12} + \alpha_d \alpha_{wp} x_{wp}^{12} + \alpha_d \alpha_{ch} x_{ch}^{12}}{r_b^{12} + r_s^{12} + x_{wp}^{12} + x_{ch}^{12}} \tag{21}$$

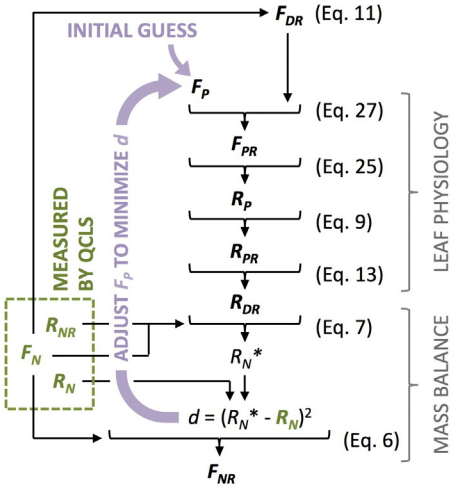

Fig. 2. Flowchart depicting numerical solution of the IFP equations.

and likewise for α_2, where

$$\alpha_d \equiv k_H^{12}/k_H^{13} \tag{22}$$

is the (equilibrium) fractionation for dissolution of CO_2. Combining Eqs. (A3) and (18)–(22) yields:

$$R_P = \frac{R_c}{\alpha_f} = \frac{1}{\alpha_d \alpha_f} \cdot \frac{c_n^{13} + \alpha_1 r_1^{12} R_P F_P^{12} + \alpha_2 r_2^{12}(R_{PR}F_{PR}^{12} + R_{DR}F_{DR}^{12})}{c_n^{12} + r_1^{12}F_P^{12} + r_2^{12}(F_{PR}^{12} + F_{DR}^{12})}, \tag{23}$$

where α_f is the fractionation factor for CO_2 fixation (Appendix B7). Replacing the ^{12}C quantities with total C quantities, as in Eq. (7), gives:

$$R_P = \frac{c_n^{13} + \alpha_2 r_2(R_{PR}F_{PR} + R_{DR}F_{DR})}{\alpha_d\alpha_f(c_n + r_1F_P + r_2F_{PR} + r_2F_{DR}) - \alpha_1 r_1 F_P}. \tag{24}$$

Inserting Eq. (9) and Eq. (13) into Eq. (24) eliminates R_{PR} and R_{DR}:

$$R_P = \frac{c_n^{13}}{\alpha_d\alpha_f(c_n + r_1F_P + r_2F_{PR} + r_2F_{DR}) - \alpha_1 r_1 F_P - \frac{\alpha_2 r_2 a_0 F_{PR}}{1+a_1F_{PR}/F_P} - \frac{\alpha_2 r_2 (F_P + a_0 F_{PR}/(1+a_1F_{PR}/F_P))F_{DR}}{\alpha_{DR}(F_P+F_{PR}+F_{DR})-F_{DR}}}. \tag{25}$$

Having obtained the desired expression relating R_P to F_P, let us go back and complete the expression for F_{PR} by inserting Eq. (18) for c_c/k_H into Eq. (8). The result is a quadratic equation for F_{PR},

$$r_2F_{PR}^2 + (r_1F_P + r_2F_{DR} + c_n)F_{PR} + F_P\Gamma_*'c_{air} = 0, \tag{26}$$

the physically meaningful root of which is always

$$F_{PR} = \frac{-(r_1F_P + r_2F_{DR} + c_n) + \sqrt{(r_1F_P + r_2F_{DR} + c_n)^2 - 4r_2F_P\Gamma_*'c_{air}}}{2r_2}. \tag{27}$$

The values of the fluxes retrieved by isotopic partitioning depend on the values of the resistances and fractionations used in the above equations. Best estimates of those resistances and fractionations based on the literature are discussed in Appendix B.

2.4. Numerical solution of the equations

With F_N, R_N, and R_{NR} measured, and using the parameterization described in Appendix B, Eqs. (7), (9), (11), (13), (25) and (27) form a system of six equations in six unknowns (F_P, R_P, F_{PR}, R_{PR}, F_{DR}, and R_{DR}), which when solved, give the desired fluxes of photosynthesis (GEP = $-(F_p + F_{PR})$) and whole-ecosystem respiration ($R_{eco} = F_{DR} + F_{NR}$). We solve this system numerically rather than analytically. The procedure, depicted in Fig. 2, is as follows:

1) Prescribe F_{DR} using Eq. (11).
2) Guess F_P.
3) Calculate F_{PR} from Eq. (27).
4) Calculate R_P from Eq. (25).
5) Calculate R_{PR} from Eq. (9).
6) Calculate R_{DR} from Eq. (13).
7) Calculate R_N from Eq. (7). Call this value R_N^*.
8) Compute $d = (R_N^* - R_N)^2$, where R_N is the measured value.
9) Repeat steps 2–8, adjusting F_P to minimize d.
10) Calculate F_{NR} from Eq. (6) using the optimized fluxes and ratios from step 9.

Care must be taken in the particulars of the minimization because the equations typically admit multiple solutions (~75% of the time) and sometimes none at all (~25% of the time). When there are multiple solutions, a plot of d *versus* F_P will reveal more than one dip to zero (within computational machine precision), but in our experience, only one of the corresponding F_P values is plausible, the others being either near zero, substantially positive (whereas uptake fluxes are defined negative), or of an absurdly large magnitude. For the temperate forest dataset used here (Section 3), the plausible value could always be selected as the most negative value less negative than $-100\,\mu mol\,m^{-2}\,s^{-1}$.

When there is no solution to the partitioning equations, due either to measurement error (most likely noise in δ_N) or to the violation of one or more assumptions, a plot of d *versus* F_P will reveal a broad minimum well above computational machine zero (e.g. 10^{-9}, well above 10^{-16}), and it is necessary to choose whether to accept that minimum as the best approximate solution or to reject the data point entirely. Rejection might seem conservative but would itself induce a bias because, as it happens, error that pushes F_P to lesser magnitudes is much more likely to cause the exact solution to vanish than is error that pushes F_P to greater magnitudes. The biases involved in accepting or rejecting best approximate solutions are described in Section 4.3.

Note that the above considerations apply equally to the previously published IFP methods, which admitted no exact solution roughly as often as did the full theory presented here.

3. Measurements

The measurements used here span May through October 2011 at the Harvard Forest Environmental Measurements Site (Goulden et al., 1996; Urbanski et al., 2007; Wofsy et al., 1993), situated in a temperate deciduous forest dominated by red oak and red maple but also including hemlock, white pine, and red pine, in Massachusetts, U.S.A. For calculations of the leaf boundary layer and mesophyll resistances, we treat all leaves at the site as oak leaves; given the sensitivity of the partitioning to these resistances (Section 4.4), this approximation should introduce a proportional error in GEP of at most a few percent.

3.1. Eddy fluxes

The isotopic CO_2 flux measurements were acquired using a quantum cascade laser spectrometer (QCLS) and have been described in detail elsewhere (Wehr et al., 2013). The sensible heat and water fluxes were measured by the long-term HF-EMS eddy

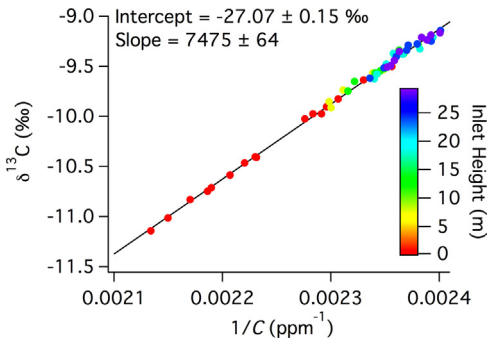

Fig. 3. An example Keeling plot used to determine the isotopic signature of non-foliar respiration through the night of May 25–26, 2011. Inlets near the ground (red) exert a dominant influence on the *y*-intercept.

flux system (Goulden et al., 1996; Urbanski et al., 2007; Wofsy et al., 1993). Flux measurements were sparse in May owing to inclement weather and associated power outages.

3.2. The isotopic signature of non-foliar respiration

We obtained the isotopic signature of non-foliar respiration, δ_{NR}, from nighttime Keeling plots (i.e. plots of δ *versus* $1/C$, in which the *y*-intercept is the respiratory source signature). For each night, we constructed a Keeling plot using all values of C and δ measured by the QCLS at all 7 sampling heights on the HF-EMS tower, including inlets at 0.2 and 1.0 m above ground (Wehr et al., 2013). An example Keeling plot from the night of May 25–26 is shown in Fig. 3. The vast majority of the variation in C and δ in the Keeling plot came from their vertical gradients rather than temporal variation. We confirmed by a simple multilayer isotopologue eddy diffusion simulation (designed specifically for our site and conditions) that the intercept of such a Keeling plot is very close to the isotopic signature of belowground respiration and is almost uninfluenced by canopy respiration. For example, if canopy respiration is 25% of the total ecosystem respiration and its signature is 4‰ different from the belowground signature, the Keeling plot intercept is still within 0.2‰ of the belowground signature. This insensitivity to canopy respiration is due to the fact that the Keeling plot intercept is dominated by the high-CO_2 measurements near the ground (as is clear from Fig. 3), which are dominated in turn by belowground-respired CO_2. Thus our Keeling plot intercepts should not be significantly contaminated by foliar respiration. The intercepts were interpolated in time using a Loess filter, rejecting extreme points, to obtain δ_{NR} for each flux measurement point.

There are two key assumptions implicit in this approach. The first is that δ_{NR} may vary from day to day but not hourly, so that it does not change significantly during the night and it does not differ systematically between night and day. This assumption is supported by our preliminary measurements of the isotopic composition of the soil surface CO_2 efflux in automated chambers at the HF-EMS, made in August 2012 (unpublished data); these measurements put an upper limit of 0.25‰ on peak-to-peak diel variation in the isotopic signature of belowground respiration (which translates into a proportional error of less than 1% in GEP retrieved by IFP), consistent with recent results in a subalpine conifer forest (Bowling et al., 2015). Previously, Betson et al. (2007) put an upper limit of about 1‰ on said variation in a boreal forest.

The second assumption is that δ_{NR} does not vary spatially, i.e. with the tower footprint. To get an indication of the impact of footprint motion on δ_{NR}, we computed the flux-weighted isotopic composition of nighttime NEE in three wind sectors chosen according to the magnitude of nighttime NEE: 0–180° (a low flux sector), 180–260° (a moderate flux sector), and 260–360° (a high flux sector). The flux weighting, which reduced the influence of highly uncertain values near zero NEE, was accomplished by taking δ_N as the slope of a linear fit to a plot of the isoflux I_N ($=\delta_N F_N$) *versus* F_N, with the fit forced through the origin. The resulting values of nighttime δ_N were: -26.8 ± 0.7‰ (0–180°), -26.0 ± 0.6‰ (180–260°), and -26.6 ± 0.3‰ (260–360°). All these values fall within one standard error of the seasonal mean δ_{NR} as determined by Keeling plots at the tower, which was -26.5 ± 0.1‰. Given the possible spread of δ_N across our three wind sectors, we estimate the uncertainty in δ_{NR} due to spatial variation at about ±0.5‰ (1 standard deviation). The uncertainty in δ_{NR} due to our Keeling plot approach is less than that. As we will see in Section 4.4, a 0.5‰ error in δ_{NR} would cause a 0.2‰ error in δ_A and a 2% error in GEP (8% in R_{eco}). A caveat regarding this directional analysis is that nighttime NEE includes foliar respiration, the influence of which is suppressed in our estimates of δ_{NR}. Nonetheless, as non-foliar respiration should be the larger component of total respiration (Wofsy et al., 1993; Xu and Griffin, 2008), spatial variation in δ_{NR} is unlikely to be significantly greater than that in nighttime δ_N.

3.3. Leaf area index

Leaf area index (LAI) is used in the calculation of the leaf boundary layer conductance (Eq. (B3)) and mesophyll conductance (Eq. (B13)), and in the parameterization of stomatal conductance when evaporation is non-negligible (Eq. (B11)). We estimate LAI here from plant area index (PAI), measured optically at several plots in the tower footprint on a monthly basis (as part of routine HF-EMS operations) and interpolated to our 40-minute time grid. We adjust observed PAI to LAI by accounting for the wood fraction and the evergreen and deciduous LAI components, as follows. True PAI is the sum of the wood area index (WAI) and the leaf area index (LAI), the latter of which is the sum of the evergreen leaf area index (ELAI) and the deciduous leaf area index (DLAI); however, as LAI increases, optically measured PAI (hereafter PAI*) approaches LAI because leaves mask branches (Breda, 2003; Kucharik et al., 1998). Thus, to a practical approximation, PAI* varies between LAI in the summer and WAI + ELAI in the winter. Accordingly, we rescale the conventional calculation of DLAI so that:

$$\mathrm{LAI} = \left(\frac{\mathrm{PAI}^*_{\max} - \mathrm{ELAI}}{\mathrm{PAI}^*_{\max} - \mathrm{PAI}^*_{\min}} \right) (\mathrm{PAI} * - \mathrm{PAI}^*_{\min}) + \mathrm{ELAI} \qquad (28)$$

where $\mathrm{PAI}^*_{\max}$ is the summertime peak PAI* (roughly equal to peak LAI) and $\mathrm{PAI}^*_{\min}$ is the wintertime minimum PAI* (roughly equal to WAI + ELAI). The second bracket in Eq. (28) is the conventional calculation of DLAI, and the first bracket is our rescaling factor. Because we do not have measurements of ELAI and WAI separately, we specify $\mathrm{ELAI} = \mathrm{WAI} = \mathrm{PAI}^*_{\min}/2$, a rough approximation. At the HF-EMS in 2011, $\mathrm{PAI}^*_{\max} = 5.1$ and $\mathrm{PAI}^*_{\min} = 1.9$, but PAI* was greater than 3 throughout the measurement period reported here.

3.4. Data filtering

Following previous work at this site (Urbanski et al., 2007), only flux measurements for which the friction velocity (u_*) exceeded 0.17 were used. In addition, for the calculation of stomatal conductance via Eq. (B9) in Appendix B, it was necessary to exclude those rare daytime measurements for which either the water flux or the leaf-air vapor pressure difference was negative (in which case there is no transpiration). For IFP, it was further necessary to exclude those rare measurements for which the stomatal conductance calculated via Eq. (B9) was negative (due to measurement noise). Finally, we restricted IFP to measurements for which PAR > 50 μE m^{-2} s^{-1} because the isotopic composition of the

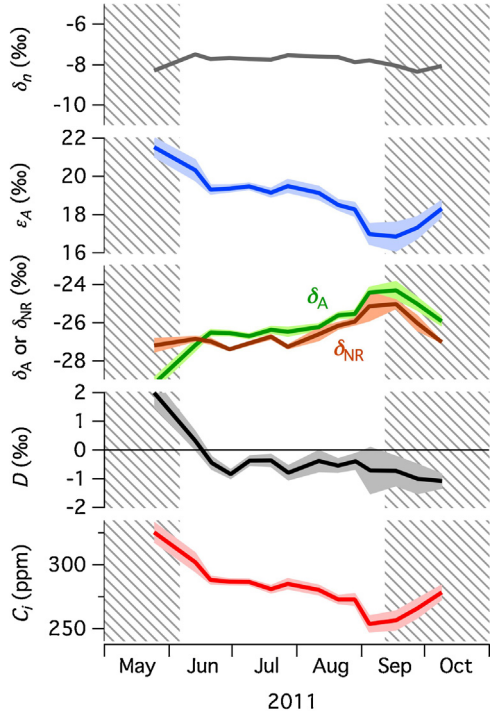

Fig. 4. Seasonal cycles of: the isotopic composition of CO_2 in the canopy airspace, δ_n; the apparent fractionation by net photosynthetic assimilation (i.e. the discrimination), ε_A; the isotopic signatures of net photosynthetic assimilation, δ_A, and non-foliar respiration, δ_{NR}; the isotopic disequilibrium, D; and the intercellular CO_2 mole fraction, C_i. The dark lines connect flux-weighted means (including all daylight hours) for each 10-day bin, except in the case of δ_{NR}, where the lines connect simple means for each bin including all nighttime hours (because δ_{NR} is derived from nighttime Keeling plots rather than daytime flux measurements). The light shaded bands around the dark lines show the standard errors in the flux-weighted means calculated according to the ratio variance approximation recommended in (Gatz and Smith, 1995) (or just the standard error in the mean for δ_{NR}), based on the variability within each bin. Hatched areas indicate periods of leaf expansion and senescence, during which some parameters used for isotopic partitioning might not be valid.

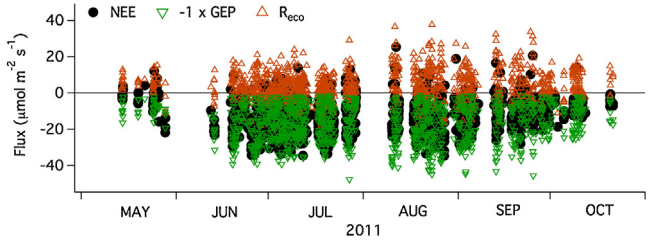

Fig. 5. Individual eddy covariance measurements of NEE (black) partitioned into GEP (green upward-pointing triangles, inverted) and R_{eco} (brown downward-pointing triangles). All partitioned flux measurements from 2011 are shown. (For interpretation of the references to color in this figure legend, the reader is referred to the web version of this article.)

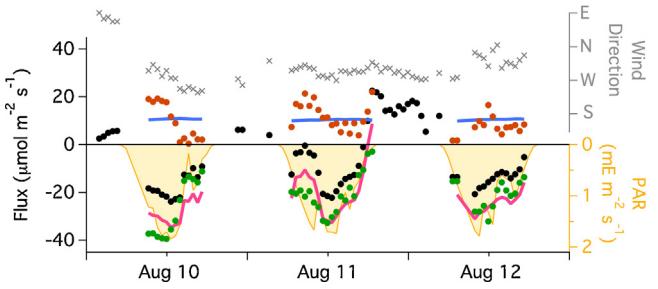

Fig. 6. NEE (black circles) and isotopically partitioned GEP (green circles, inverted) and R_{eco} (brown circles) over 3 days in August 2011, smoothed to 2 h (i.e. 3 points). Also shown are wind direction (crosses, top panel), PAR (yellow shading, inverted), and GEP (pink lines) and R_{eco} (blue lines) estimated by standard partitioning based on nighttime NEE and temperature. Missing points were filtered out by one of the criteria discussed in Section 3.4. (For interpretation of the references to color in this figure legend, the reader is referred to the web version of this article.)

photosynthetic flux becomes noisy as that flux approaches zero (and is undefined when that flux is zero).

4. Results and discussion

4.1. Demonstration: the seasonal patterns of isotopic discrimination and disequilibrium

In order for IFP to work, the isotopic signature of net photosynthetic assimilation, δ_A, must be distinct from (i.e. out of equilibrium with) that of non-foliar respiration, δ_{NR}. For an individual eddy flux measurement, that is almost always the case because of the relatively large (several ‰) diurnal variation of δ_A and the relative constancy (<0.25‰) of δ_{NR}. In addition, our results (Fig. 4) confirm that even at the seasonal timescale, there is a small but distinct isotopic disequilibrium ($D = \delta_{NR} - \delta_A$), stable at roughly −0.5‰ through most of the growing season but with high values (>0) at the start and slightly low values (−1‰) at the end. The sign (which is opposite to that expected from the Suess effect), approximate magnitude, and relatively high early-season values of D are consistent with recent measurements in a subalpine conifer forest (Bowling et al., 2014), although those measurements indicated a late-season increase in D rather than the slight decrease found here. Several plausible explanations for persistent negative D were discussed in that study, including post-photosynthetic fractionation leading to sequestration of isotopically enriched carbon in wood or soil (Bowling et al., 2014). Note that none of the systematic uncertainties considered in Section 4.4 is likely to account for a bias in D of 0.5‰.

Though offset by the disequilibrium, the seasonal pattern of δ_{NR} (which describes the ecosystem carbon output) closely matches that of δ_A (which describes the ecosystem carbon input) with no resolvable time lag (Fig. 4), indicating that most respired carbon has resided in the ecosystem for less than a week. The match between these patterns also substantiates the IFP results because δ_A is an output of IFP while δ_{NR} is an independent measurement (Section 3.2). (Although the IFP calculation takes δ_{NR} as an input, the value of δ_A determined by IFP is hardly influenced by the value of δ_{NR}: a 0.5‰ change in δ_{NR} causes only a 0.1‰ change in δ_A, as shown in Section 4.4).

Fig. 4 also shows the close correspondence of the apparent fractionation by net photosynthetic assimilation, ε_A (commonly called discrimination), and the intercellular CO_2 mole fraction, consistent with the basic idea of stomatal influence expressed in Eq. (4).

4.2. Demonstration: precision and ecosystem heterogeneity

We partitioned 1042 independent NEE measurements over the 2011 growing season (Fig. 5), but to reveal the characteristics of IFP, we focus on 3 illustrative days in August 2011 (Fig. 6). We note two broad features of interest.

First, the variability in daytime R_{eco} from IFP is similar in magnitude and character to that in nighttime NEE, suggesting that the precision of the isotopically partitioned fluxes is similar to that of NEE itself. Indeed, taking all July measurements together, the standard deviation of daytime R_{eco} to the southwest of the tower was 5.8 μmol m^{-2} s^{-1}, compared to 5.3 μmol m^{-2} s^{-1} for July nighttime NEE in the same quadrant. We conclude that the variability in daytime R_{eco} and GEP derived almost entirely from

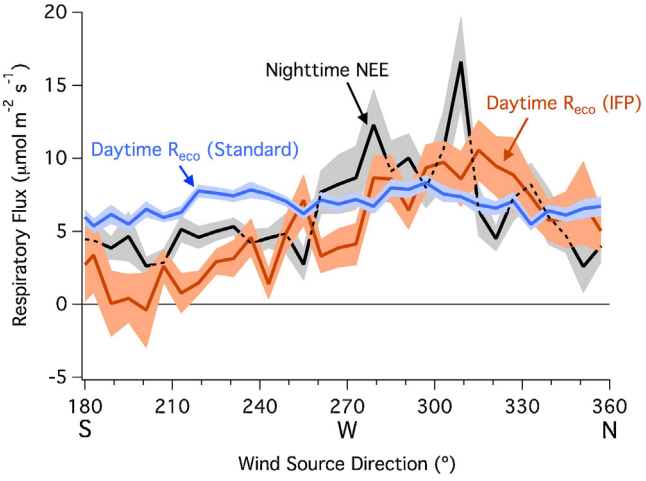

Fig. 7. Nighttime NEE (black), daytime R_{eco} estimated by isotopic flux partitioning (brown), and daytime R_{eco} estimated by standard partitioning based on nighttime NEE and temperature (blue) *versus* wind direction, over the entire growing season. Dark lines are bin means while light shaded regions indicate ±1 standard error in the mean based on variability within the bin. (For interpretation of the references to color in this figure legend, the reader is referred to the web version of this article.)

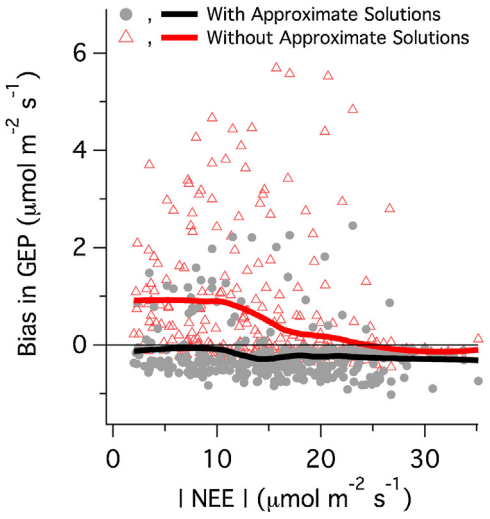

Fig. 8. Bias in GEP resulting from normally distributed measurement error in δ_N coupled with the nonlinear nature of the partitioning equations, as a function of the absolute magnitude of NEE, when best approximate solutions are included (gray circles, black line) or excluded (pink triangles, red line). The points are bias estimates for each of the individual flux measurements in July, 2011, and the lines are smoothings *versus* the absolute magnitude of NEE, made using a Loess filter. (For interpretation of the references to color in this figure legend, the reader is referred to the web version of this article.)

variability in measured NEE rather than from the isotopic partitioning.

Second, the measured respiration—day or night—depends strongly on wind direction, a coarse indicator of the tower sampling footprint. The dependence is strong (Fig. 7): certain areas to the northwest of the tower exhibited respiratory fluxes that were on average 3 times greater than those in areas to the southwest. This directional variation in respiration violates the eddy covariance assumption of a horizontally homogeneous ecosystem (which cannot be fully satisfied at any real site) and therefore probably induces errors in NEE. Additionally, it causes further (and likely larger) errors in standard NEE partitioning because that partitioning is based on 4- or 6-day regression windows and therefore blends the different tower footprints together. Thus standard R_{eco} is virtually flat through the day (Fig. 6), and the variations in NEE due to footprint motion are mistakenly attributed entirely to GEP—which therefore behaves erratically with respect to environmental drivers, as is most evident on the morning of August 11 in Fig. 6, when standard GEP is strongly anti-correlated with PAR.

IFP, on the other hand, captures the directional variation in respiration because it partitions each flux measurement independently. From the perspective of one interested in whole-ecosystem (i.e. spatially integrated) R_{eco} and GEP, IFP correctly partitions the meteorological noise in NEE while standard partitioning does not. IFP reveals that GEP was also greater to the northwest than to the southwest, but the proportional variation was less than 20% (not shown).

Standard partitioning based on light-response curves (Lasslop et al., 2010) can be even more severely corrupted by footprint motion because the method interprets footprint-related variations in measured daytime NEE as being light-related, and can thereby arrive at unrealistic light-response curves. In the days surrounding August 11, for example, this method exaggerated GEP and R_{eco} by a factor of 2, putting R_{eco} at about 35 μmol m^{-2} s^{-1} all day (not shown). More subtle errors of the same kind would bias estimates of GEP and R_{eco} without being detectible, absent the isotopic flux measurements.

We should point out that August 11 is the most extreme day in the dataset in terms of footprint motion and of disagreement between standard and isotopic partitioning; August 10 and 12 are more typical of the northwest quadrant.

4.3. Biases due to the structure of the equations

Because the partitioning equations are nonlinear, normally distributed error in the measured variables can translate into skewed error and therefore bias in GEP. For the instrumentation that acquired the data used here (Section 3), the only measured variable with non-negligible random error was δ_N, and the bias due to that error turned out to be negligible. We estimated the bias as follows.

For each eddy flux measurement in July, we determined the response of GEP to the value of δ_N (all else being equal) by rerunning the partitioning calculation using a range of values of δ_N rather than the actual measured value. The shape of this response curve depends on other variables such as the magnitude of NEE, so that it varies from one eddy flux measurement to the next. We then used the resulting response function for each eddy flux measurement to map normally distributed error in δ_N onto GEP for that measurement. We centered the distribution of error in δ_N on an approximate true δ_N estimated as the flux-weighted average of all δ_N measurements within ±2 h of the measurement under consideration, and we set the standard deviation of the error in δ_N as $14.2(\mathrm{NEE}^{-0.955}) + 0.215$, which is a close description of the random instrument error based on the characterization method detailed in Wehr et al. (2013); as NEE increases, error in δ_N decreases. Finally, for each flux measurement, we computed the bias as the difference between the mean of the resulting GEP distribution and the 'true' GEP calculated from the approximate true δ_N.

The resulting bias estimates when including or excluding best approximate solutions to the partitioning equations (Section 2.4) are plotted *versus* the absolute magnitude of NEE in Fig. 8. The bias estimates for individual eddy flux measurements are subject to variability associated with environmental conditions as well as with error in our approximate true δ_N, and so we have used a Loess filter to smooth them *versus* the magnitude of NEE. The smoothed curves show that the bias in GEP when including best approximate solutions is between zero and −0.3 μmol m^{-2} s^{-1} for all values of NEE; the overall mean is −0.2 μmol m^{-2} s^{-1} (−1% of the July daytime mean GEP). When excluding approximate solutions, GEP is biased positively at low magnitudes of NEE by up to 1 μmol m^{-2} s^{-1},

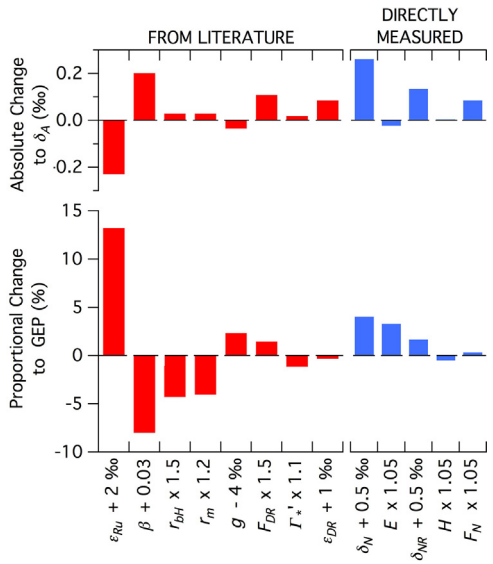

Fig. 9. Sensitivity analyses: responses of growing season mean δ_A and GEP to adjustments in various IFP input parameters (red) and measured quantities (blue). (For interpretation of the references to color in this figure legend, the reader is referred to the web version of this article.)

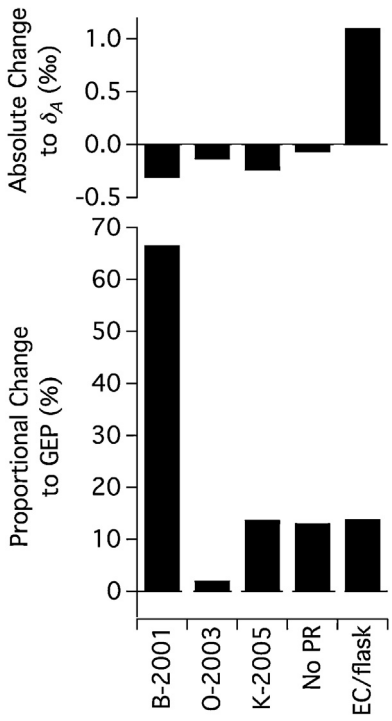

Fig. 10. Sensitivity analyses: responses of growing season mean δ_A and GEP to three simplifications of the IFP theory (B-2001 = Bowling et al., 2001; O-2003 = Ogée et al., 2003; K-2005 = Knohl and Buchmann, 2005), to the neglect of photorespiration in particular (No PR), and to use of the EC/flask approximation to the isotopic composition of NEE (EC/flask).

with an overall mean of + 0.4 μmol m^{-2} s^{-1} (+2% of the July daytime mean GEP). We therefore chose to accept best approximate solutions, thereby reducing bias and allowing the partitioning of more flux measurements.

Note that we have been considering random measurement error rather than total variability: as discussed in Section 4.2, there is large variability in measured NEE that is responsible for most of the variability in the retrieved fluxes, but most of that variability is not erroneous from the perspective of IFP, because it is caused by changes in the flux tower sampling footprint and, during the day, by changes in cloud cover—both of which affect the real fluxes of CO_2, water, and heat observed at the tower.

4.4. Systematic uncertainties

Because IFP depends on the complex interaction of many input parameters, we quantified its systematic uncertainty in terms of the sensitivity of whole-season mean GEP and δ_A to adjustment of each input parameter, all else being equal. The results are reported in Fig. 9, which includes each of the substantially uncertain input parameters described in Appendix B (e.g. the fractionation by Rubisco, ε_{Ru}) as well as: the rates and signatures of photorespiration and foliar daytime 'dark' respiration; the measured isotopic signature of non-foliar respiration; the measured isotopic composition of NEE; and the measured eddy fluxes of CO_2, water vapor, and sensible heat. Adjustments of the input parameters also affected the diurnal and seasonal patterns of GEP and δ_A somewhat, but the impact on their means was dominant. The magnitude of each variable's adjustment was chosen in the spirit of the standard error; that is, we judged that errors of the chosen magnitudes were fairly probable but errors of more than twice those magnitudes were improbable. Unfortunately, the literature usually presents no means for a more rigorous approach.

The bases for our judgments were as follows: ε_{Ru} + 2‰ and β + 0.03, the distributions of published values across (a limited number of) species; $r_{bH} \times 1.5$, the uncertainty reported in McNaughton and Hurk (1995) for the amalgamated coefficient 150 in Eq. (B3); $r_m \times 1.2$, the uncertainty reported in Warren and Dreyer (2006); g – 4‰, the range of values reported in Tcherkez (2006) for the photorespiratory fractionation f and for fractionation by glutamate decarboxylase (this adjustment is negative because the preferred value is at the top of the reported range); $\Gamma_*' \times 1.1$, the discrepancy between the measurements of Jordan and Ogren (1984) and Brooks and Farquhar (1985); $F_{DR} \times 1.5$, estimates of foliar dark respiration (Xu and Griffin, 2008) and of its inhibition by sunlight (Atkin et al., 1998; Hurry et al., 2005; Pärnik et al., 2007); ε_{DR} + 1‰, the uncertainty reported in Tcherkez et al. (2010) (but those measurements were for sunflower); δ_{NR} + 0.5‰, our determination of spatial heterogeneity surrounding the EMS tower (Section 3.2). For the flux measurements, we arbitrarily adjusted the values up by 5%, though such errors are not particularly likely. For δ_N, we arbitrarily adjusted the value up by 0.5‰, in keeping with δ_{NR}. In the case of the water flux E, the error could be imagined as methodological or as due to the presence of evaporation in the total water flux. The parameters are ordered in the figure according to the magnitude of the effect on GEP.

Previous IFP studies have stressed r_s and r_m as leading sources of uncertainty (Bowling et al., 2001; Knohl and Buchmann, 2005; Ogée et al., 2003; Zobitz et al., 2008). Although IFP is highly sensitive to r_s, it does not appear in Fig. 9 because it is derived from other parameters in the figure (E, H, r_{bH}, r_e, e_a, and T_a). And although IFP is also sensitive to r_m, Fig. 9 indicates that the parameters contributing the greatest uncertainty to GEP are the fractionation by Rubisco ε_{Ru} and the proportion of carboxylation done by PEP-carboxylase β, both of which concern the isotopic fractionation by carboxylation and have never before been considered as a source of error. The leaf boundary layer resistance r_{bH} is also important. The uncertainties associated with the rates and isotopic signatures of photorespiration and daytime 'dark' respiration are less than a few percent of GEP – much smaller than the error induced by neglecting photorespiration entirely (see Fig. 10). Combining all the systematic literature parameter uncertainties in Fig. 9 in a simple sum-of-squares error approach gives an overall proportional systematic uncertainty in GEP of ±17%. If the fractionation by carboxylation (ε_{Ru} and β)

were known precisely, that uncertainty would drop to ±7%. This approach assumes that the parameters are non-interacting, which is not quite true. For δ_A, the overall absolute systematic uncertainty is ±0.3‰ (±0.1‰ if ε_{Ru} and β were known precisely).

The systematic uncertainty associated with the big-leaf canopy approximation underlying the IFP equations in Section 2 (and all simplifications thereof) cannot be quantified without knowing how the sources and sinks of $^{13}CO_2$, $^{12}CO_2$, light, water, and heat are distributed throughout the canopy. Leaf-level measurements distributed through the canopy would be valuable for testing the big-leaf approximation and implementing a multi-leaf version of IFP. Error due to this approximation might be correlated with PAR and time of day or season via the sun angle and the diffuse light fraction, but with sufficient data, these variations could be constrained by analyzing periods of completely diffuse light and identical canopy structure.

In addition to estimating systematic uncertainties, we can use sensitivity analyses to ask what is gained by the extended theoretical framework presented here. Thus in Fig. 10, we present the biases (relative to the full model presented here) induced in GEP and δ_A by using the simplified theoretical formulations of Bowling et al. (2001), Ogée et al. (2003), and Knohl and Buchmann (2005) (but always using the same stomatal conductance, determined by our method described in Appendix B4). We also present the bias induced by neglecting photorespiration in particular. The original isoflux-based IFP formulation (Bowling et al., 2001), which lacked boundary layer and mesophyll resistances, gives a bias of +67% of GEP (i.e. GEP was systematically too high compared to what would be estimated by the approach here), while the more recent formulations (Knohl and Buchmann, 2005; Ogée et al., 2003) give biases of +2% and +14% of GEP. All previous formulations neglect photorespiration, which in itself biases GEP by +13%, but the overall biases in the more recent formulations are similar to or less than +13% because other approximations and errors fortuitously balance the neglect of photorespiration for this dataset; for example, neglecting foliar daytime 'dark' respiration biases GEP by −3% (not shown). Each simplified formulation also gives a bias of between −0.1 and −0.3‰ in δ_A. Because none of the major systematic uncertainties in the full theory (those related to ε_{Ru}, β, r_{bH}, and r_m) is removed by any of the simplifications, the full theory is preferable—at least when applied to a deciduous oak forest. (Assigning a parameter a value well outside the range of uncertainty in that parameter, e.g. $\Gamma_*' = 0$, does not change the uncertainty; it merely guarantees some minimum bias associated with that parameter.)

The final column in Fig. 10 shows the biases resulting from the EC/flask approximation (Bowling et al., 2001) used by most IFP studies (Bowling et al., 2001; Knohl and Buchmann, 2005; Lai et al., 2003; Ogée et al., 2003; Zobitz et al., 2008) in place of direct measurements of the isotopic flux. Our method for simulating the EC/flask method has been described elsewhere (Wehr et al., 2013). For our temperate forest dataset, the EC/flask approximation biases GEP by +14% and biases δ_A by +1.1‰, which is greater than the seasonal mean isotopic disequilibrium and so non-negligible. We therefore recommend that direct flux measurements be used instead of the EC/flask approximation.

The bias induced in the diel cycle of non-foliar respiration (F_{NR}) by three of the simplifying formulations (Bowling et al., 2001; Knohl and Buchmann, 2005; Ogée et al., 2003) is presented in Fig. 11. Because the respiratory flux is smaller than the photosynthetic flux, the +14% bias in GEP associated with the formulation in Knohl and Buchmann (2005), for example, corresponds to a more than doubling of midday non-foliar respiration. The results from the full theory suggest, intriguingly, that daytime ecosystem respiration is less than nighttime ecosystem respiration, consistent with leaf-level studies reporting that foliar respiration is inhibited by light (Heskel et al., 2013). However, confirmation of that possibility at

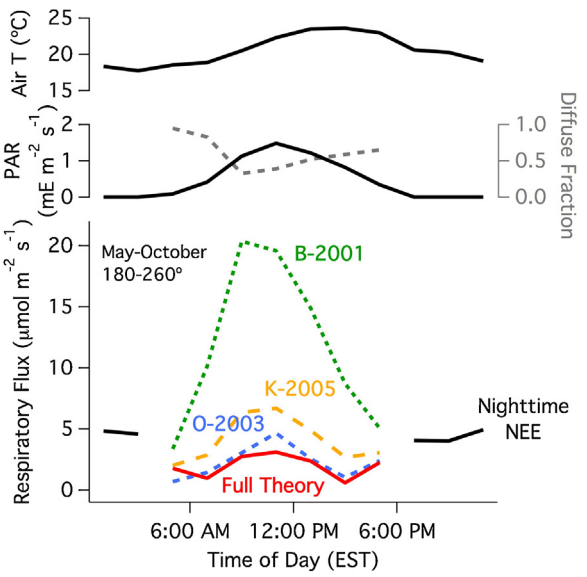

Fig. 11. Growing season median diel cycles of non-foliar respiration to the southwest of the flux tower, as determined by the present IFP formulation (solid line) and the three previously published simplifications from Fig. 10 (dotted and dashed lines), along with nighttime NEE. Also shown for comparison are: growing season median air temperature, PAR (solid black line), and diffuse light fraction (dotted grey line).

the ecosystem scale would require a reduction in the systematic uncertainty of the partitioning, to less than about 1 μmol m^{-2} s^{-1} (~6% of GEP), which would depend in particular on reducing the uncertainties associated with the big-leaf approximation and the isotopic fractionation by carboxylation. Those uncertainties could both be reduced by feasible site-specific leaf-level measurements, as could uncertainty in the mesophyll conductance.

Even without a reduction in those *a priori* uncertainties, IFP can be used to study temporal patterns with much greater certainty than means or sums, because the systematic uncertainties in Fig. 9 have only minor (and quantifiable) effects on many temporal patterns in GEP and δ_A. As noted above, with sufficient data, even the as-yet unquantifiable effect of the big-leaf approximation can be rendered time-invariant by restricting analysis to periods of highly diffuse light and nearly identical canopy structure. It may thereby prove possible to constrain the overall uncertainty in IFP *a posteriori* by validation against infrequent instantaneous or time-integrated estimates of GEP or daytime R_{eco}.

5. Conclusion

We have presented an extended formulation of isotopic flux partitioning from which all previously published formulations can be derived as simplifying approximations, and demonstrated the method using data from a temperate deciduous forest. The statistical uncertainty in GEP and R_{eco} was found to be negligible compared to variability in NEE itself, while the assessable systematic uncertainty was ±17% of gross ecosystem production. Systematic uncertainty in the isotopic composition of canopy net photosynthates was ±0.3‰. Neglect of photorespiration in previously published formulations was found to bias GEP high (by 13%), but that bias was sometimes offset by other approximations and errors. Some bias due to the approximation of the canopy as a 'big leaf' should be common to this and all previous formulations but cannot be estimated at present, for lack of data describing the canopy heterogeneity.

The partitioning revealed that the isotopic signature of ecosystem non-leaf respiration closely tracked the signature of carbon

supply from the leaves, indicating that most respired carbon had resided in the ecosystem for less than a week. The disequilibrium between carbon input and output was stable on the seasonal timescale through most of the growing season, agreeing with recently published measurements but contradicting the prevalent idea that the disequilibrium results from the Suess effect.

Our results illustrated a key practical advantage over standard non-isotopic partitioning, which is the ability to partition individual flux measurements and thereby reduce errors and biases due to changes in the flux tower sampling footprint. The fundamental advantage, however, is that isotopic flux partitioning does not prescribe the behaviors of ecosystem-scale photosynthesis or respiration, which one is therefore free to discover. In the temperate forest studied here, isotopic partitioning suggested that daytime ecosystem respiration was less than nighttime ecosystem respiration, consistent with inhibition of leaf respiration by light, though confirmation of that possibility would require a reduction in the systematic uncertainty of the partitioning.

The measurements most likely to reduce that uncertainty are measurements of the fractionation by carboxylation and of the mesophyll resistance, in relevant species, and measurements constraining canopy heterogeneity sufficiently to enable a multi-leaf isotopic partitioning framework. Regardless of its systematic uncertainty, isotopic flux partitioning allows for the investigation of temporal patterns and thereby offers a unique window into the controls on ecosystem photosynthesis and respiration. Isotopic partitioning would be especially powerful in concert with complementary and potentially corroborating methods such as H_2O–CO_2 correlation analysis (Scanlon and Kustas, 2010), carbonyl sulfide flux analysis (Billesbach et al., 2014; Wohlfahrt et al., 2011), sun-induced fluorescence (Joiner et al., 2013), soil chambers, and leaf chambers.

Acknowledgements

This research was supported by the U.S. Department of Energy, Office of Science, Terrestrial Ecosystem Science (TES) Program (Award #DE-SC0006741). The Harvard Forest Environmental Measurements Site infrastructure is a component of the Harvard Forest Long-Term Ecological Research (LTER) site, supported by the National Science Foundation (NSF), and is additionally supported by the DOE TES program.

Appendix A. Definitions

The conductance g ($m\,s^{-1}$) and resistance $r \equiv 1/g$ ($s\,m^{-1}$) to CO_2 transport between point z_1 and point $z_2 > z_1$ are defined by Fick's law of diffusion:

$$F \equiv -g(c(z_2) - c(z_1)), \tag{A1}$$

where F is the net flux ($mol\,m^{-2}\,s^{-1}$) in the positive z direction and $c(z)$ is the concentration ($mol\,m^{-3}$) at point z. Because we employ the convention that fluxes into the atmosphere are positive, the photosynthetic flux is negative.

The relative isotopic composition δ of a substance or flux is defined as:

$$\delta \equiv \frac{R}{R_{VPDB}} - 1, \tag{A2}$$

where R is the ratio of ^{13}C atoms to ^{12}C atoms in the substance or flux, and R_{VPDB} is the ratio of ^{13}C atoms to ^{12}C atoms in the Vienna Pee Dee Belemnite standard material. We follow Griffis et al. (2004) in using the value $R_{VPDB} = 0.0111797$, but the choice of R_{VPDB} has no effect on IFP so long as it is consistent.

The isotopic fractionation factor α (also called the isotope effect) for an irreversible process such as diffusion or carboxylation is defined as:

$$\alpha \equiv \frac{k^{12}}{k^{13}} = \frac{R_{source}}{R_{product}}(\text{for a reaction}) = \frac{g^{12}}{g^{13}}(\text{for diffusion}), \tag{A3}$$

where k^{12} and k^{13} are the isotope-specific rate constants for the process.

The isotopic fractionation ε is defined as:

$$\varepsilon \equiv \alpha - 1 = \frac{\delta_{source} - \delta_{product}}{1 + \delta_{product}}(\text{for a reaction}), \tag{A4}$$

and should not be approximated as $\delta_{source} - \delta_{product}$ (as it has been in all IFP studies to date). That approximation induces a proportional error in ε equal to $\delta_{product}$, which is about −30‰ in the case of the apparent fractionation of net photosynthesis. The corresponding absolute error is −0.7‰, which is not negligible. Moreover, the exact definition, Eq. (A4), is tractable. Note that the alternative definitions $\alpha \equiv R_{product}/R_{source}$ and $\varepsilon \equiv 1 - \alpha$ have also been used (e.g. Lee et al., 2009), and were acknowledged by Farquhar et al. (1989), but only the definitions used here are consistent with Farquhar et al. (1989) and Coplen (2011).

Appendix B. Values for the resistances, fractionations, and other input parameters

The published literature provides values or empirical formulae for all those parameters that are required to solve our system of equations but that we do not measure. In this appendix, we describe the best estimates available for each. In Section 4.4, we test the sensitivity of IFP to these parameters according to their estimated uncertainties.

B.1. Canopy CO_2 concentration, vapor presssure, and temperature

The concentration and isotopic composition of CO_2 in the canopy (c_n and δ_n) are determined from the same measurements used to determine the canopy CO_2 storage (iso-)flux for the calculation of F_N and δ_N (Wehr et al., 2013). In particular, c_n and δ_n are averages of measurements at 12, 18, and 24 m on the flux tower, which span the region of maximum light absorption determined by G.G. Parker in 1998 (unpublished data), and which were meant to represent the region of peak photosynthetic assimilation.

From the within-canopy and above-canopy CO_2 measurements, it is possible to define a turbulent eddy transport resistance r_e by assuming that turbulent eddy transport functions as a gradient-driven diffusion process (Raupach and Thom, 1981), and treating the canopy as a single thin layer. In that situation, one can use Fick's Law, Eq. (A1), to write:

$$c_n = c_a + r_e F_e \tag{B1}$$

where F_e is the CO_2 eddy flux (i.e. without storage). Applying the same resistance r_e to heat and water vapor (i.e. assuming the same eddies transport all scalar quantities indiscriminately, with differences in their source/sink distributions neglected, in keeping with a single-thin-layer canopy) allows us to calculate the canopy airspace temperature T_n and vapor pressure e_n, which will be necessary to calculate leaf temperature and thence stomatal resistance in Eqs. (B8)–(B9), below.

The sign of r_e calculated from Eq. (B1) was sometimes negative, indicating counter-gradient transport (Raupach and Thom, 1981), which we did not forbid. To reduce the impact of sampling noise in the canopy CO_2 concentrations (which are only measured for a few minutes out of every 40 min), we smoothed r_e to 2 h. By using canopy CO_2 measurements from the tower, we are assuming that

the flux-gradient relationships at the tower are the same as those in the eddy flux sampling footprint at the same moment in time; some statistical error should be associated with this assumption, and possibly some systematic error as well.

B.2. Leaf boundary layer resistance

The leaf boundary layer resistance r_b varies with leaf size, shape, orientation, distribution, and density, as well as with wind speed and with the relative importance of forced and free convection near the leaf surface. It has been studied both in wind tunnels and in the field, but owing to the complexities of its spatial and temporal variability, it remains only roughly predictable, with models requiring empirical adjustments (Massman, 1999; McNaughton and Hurk, 1995; see Schuepp, 1993). The most reasonable formulation for r_b, in our estimation, is that of McNaughton and Hurk (1995). It begins with the Pohlhausen equation for heat transfer to or from a flat plate (see Schuepp, 1993), which gives, for double-sided transfer:

$$r_{bH} = 150\sqrt{\frac{L}{u}} \tag{B2}$$

where r_{bH} is the boundary layer resistance to heat transfer (different from the corresponding resistance to CO_2 transfer, as explained below), L is the plate dimension (m), u is the wind speed ($m\,s^{-1}$) just outside the boundary layer, and the amalgamated constant 150 has units of $s^{½}\,m^{-1}$. McNaughton and Hurk (1995) then make assumptions concerning the variation of wind speed and heat flux with height in order to obtain a suitable flux-weighted average boundary layer resistance to apply to the big-leaf canopy. Following the derivation in McNaughton and Hurk (1995) except in retaining u and avoiding the unhelpful division by u_*, we obtain:

$$r_{bH} = \frac{150}{\mathrm{LAI}}\sqrt{\frac{L}{u_h}}\int_0^1 \exp\left[\frac{\alpha}{2}(1-\zeta)\right]\phi(\zeta)\mathrm{d}\zeta \tag{B3}$$

where LAI is the leaf area index, L is now the characteristic leaf dimension (we use 0.1 m, typical for our site), u_h is the mean wind speed at the top of the canopy, ζ is height divided by canopy top height, $\varphi(\zeta)$ is the vertical profile of the heat source normalized such that $\int_0^1 \varphi(\zeta)\mathrm{d}\zeta = 1$, and α is the extinction coefficient (not a fractionation factor) for the assumed exponential wind profile:

$$\frac{u(\zeta)}{u_h} = \exp[\alpha(\zeta - 1)]. \tag{B4}$$

The wind speed at the top of the canopy can be obtained from Eq. (B4) with ζ set to correspond to flux measurement height a:

$$u_h = \frac{u_a}{\exp\left[\alpha\left(\frac{a}{h} - 1\right)\right]}, \tag{B5}$$

where h is the canopy top height. For canopies with leaf area indices of 0.6, 2, 4, and 9, McNaughton and Hurk (1995) suggest $\alpha = 1$, 2, 3, and 4, respectively, which corresponds to the exponential relationship $\alpha = 4.39 - 3.97\exp(-0.258 \cdot \mathrm{LAI})$, which we use to calculate α for our site. From late June through the end of August, while $5.0 < \mathrm{LAI} < 5.1$, we obtain $\alpha = 3.3$. For $\varphi(\zeta)$, we replace the assumptions in McNaughton and Hurk (1995) with the assumption that $\varphi(\zeta)$ is identical to the normalized profile of light absorption, which was measured at our site by G. G. Parker in 1998 (unpublished data). We adjust $\varphi(\zeta)$ to account for diel and seasonal variation in the solar zenith angle, which has a small (~20%) effect on r_{bH} at dawn and dusk but a negligible effect on IFP. The integration over the assumed vertical profiles of wind and heat flux in Eq. (B3) is our only departure from the assumption of a big-leaf canopy; the flux-weighted average r_{bH} obtained from Eq. (B3) is assumed to apply to all leaves equally.

The boundary layer resistances for heat (r_{bH}), CO_2 (r_b), and water vapor (r_{bV}) are related by (see Hicks et al., 1987):

$$r_b = N\left(\frac{Sc}{Pr}\right)^n r_{bH} \tag{B6}$$

$$r_{bV} = N\left(\frac{Sc_V}{Pr}\right)^n r_{bH} \tag{B7}$$

where Sc is the Schmidt number for CO_2 (≈1.05), Sc_V is the Schmidt number for water vapor (=Sc/1.57), Pr is the Prandtl number for air (≈0.71), $N = 1$ for amphistomatous leaves (i.e. leaves with stomata on both sides of the leaf, so that heat, water, and CO_2 are all transferred from both sides), and $N = 2$ for hypostomatous leaves (i.e. leaves with stomata predominantly on the underside of the leaf, so that heat is transferred from both sides while water and CO_2 are transferred from only one side). The red oak and red maple trees that dominate our Harvard Forest site are hypostomatous ($N = 2$). The empirical exponent n accounts for the fact that transfer through the boundary layer is partly turbulent and is assigned the approximate value 2/3, applicable to most gases (Hicks et al., 1987; Lamaud et al., 1994). The constant 1.57 relating Sc_V to Sc is the ratio of the binary diffusion coefficient of H_2O in air to that of CO_2 in air, as determined from their molecular masses and the molecular mass of air.

Previous IFP studies that considered the boundary layer (Billmark and Griffis, 2009; Knohl and Buchmann, 2005; Ogée et al., 2003; Zobitz et al., 2008) calculated the boundary layer resistance as a function of a constant Stanton number B (i.e. $r_{bH} = 1/u_*B$), which is not a simplification but rather a misinterpretation. The Stanton number is a dimensionless number representing the ratio of the heat flux into a fluid to the thermal capacity of the fluid, and is defined in general as $B \equiv h/\rho_a C_P u \equiv 1/r_{bH}u$, where h is the heat transfer coefficient ($W\,m^{-2}\,K^{-1}$) and u is the fluid velocity ($m\,s^{-1}$). Owen and Thomson (1963) proposed that the characteristic wind speed in the canopy should be u_* and thereby *defined* the Stanton number for all subsequent canopy exchange literature. Thus $r_{bH} = 1/u_*B$ does not express a proportionality between r_{bH} and u_*; B is merely a dimensionless form of r_{bH} that varies between sites, with time, and even with u_* (Massman, 1999; McNaughton and Hurk, 1995; Schuepp, 1993). For typical daytime conditions, B as calculated for our site based on the model of McNaughton and Hurk (1995) (Appendix B2) varies roughly between 1/8 and 1/2 and is nearly inversely proportional to u_*. Under the same conditions, r_{bH} itself only varies between about 8 and 12 $s\,m^{-1}$. Thus, assuming a constant r_{bH} would be more accurate than assuming a constant B.

B.3. Leaf temperature

Given r_{bH}, and assuming that the internal leaf temperature T_L (K) is the same as the leaf surface temperature, Fick's Law (Eq. (A1)) for thermal diffusion gives

$$T_L = \frac{Hr_{bH}}{\rho_a C_p} + T_n \tag{B8}$$

where H is the net heat flux ($W\,m^{-2}$), T_n is the canopy airspace temperature (K), ρ_a is the density ($kg\,m^{-3}$) of air, and C_p is the specific heat capacity ($J\,kg^{-1}\,K^{-1}$) of (wet) air.

B.4. Stomatal resistance

The stomatal resistance to CO_2, derived from the stomatal resistance to water vapor r_{sV}, is a highly influential parameter in IFP, since it is among the most significant and most variable of the resistance terms that set the isotopic fractionation by photosynthesis. When the measured net water vapor flux E ($mol\,m^{-2}\,s^{-1}$) is entirely transpiration, i.e. when evaporation from and condensation onto

soil and canopy surfaces is negligible, r_{sV} can be obtained from E once r_e, r_{bV}, and T_L have been calculated. Assuming that air inside the leaf is saturated with water vapor, Fick's Law (Eq. (A1) again) for diffusion of water vapor gives

$$r_{sV} = \frac{e_{SAT}(T_L) - e_n}{RT_nE} - r_{bV} \tag{B9}$$

where $e_{SAT}(T_L) = e_i$ is the saturation vapor pressure (Pa) at temperature T_L, e_n is the vapor pressure (Pa) in the canopy airspace, and $R = 8.315\,\mathrm{J\,mol^{-1}\,K^{-1}}$ is the molar gas constant (not an isotope ratio here). The stomatal resistances to H_2O and CO_2 are related by $r_s = 1.57 r_{sV}$ and the saturation vapor pressure is given by the following empirical formula (World Meteorological Organization, 2008):

$$e_{SAT}(T) = 611.2 \exp\left(\frac{17.62(T - 273.15)}{T - 30.03}\right) \tag{B10}$$

with T in Kelvin (note that this formula is provided in hPa and °C in the cited source).

Unfortunately evaporation is often non-negligible at the HF-EMS; evaporation from soil and canopy surfaces contributes substantially to the measured water flux but has no bearing on stomatal conductance, so that r_s from Eq. (B9) is often an underestimate. Canopy surface wetness can result in large evaporative water fluxes but typically lasts less than a few daylight hours after the cessation of rain or dew, a fact confirmed by the direct leaf surface water measurements of Klemm et al. (2002) as well as by our own simple experiment. Our experiment consisted of thoroughly wetting a few isolated leaves placed under an awning on a cool (18 °C), completely overcast day, with the leaf exposed to only 50% of the sky and with rain continuing to fall around (but not on) the leaf; even under these unfavorable conditions, all water had evaporated from the leaf surface within about 3 h.

Soil and ground surface water usually results in smaller evaporative fluxes but is longer lived, lasting a day or two after a large rain in hot, dry periods (e.g. late July 2011) and several days or more after a large rain in cold, wet periods (e.g. May 2011).

Our approach to calculating g_s in periods with non-negligible evaporation is adapted from Knohl and Buchmann (2005): a function is fit to EC-derived g_s in periods with negligible evaporation and used to extrapolate g_s into wet periods. For the function, Knohl and Buchmann (2005) used a stomatal conductance model (Collatz et al., 1991) in which g_s depends on the net photosynthetic assimilation flux F_A, the CO_2 molar mixing ratio to dry air at the leaf surface, and the relative humidity at the leaf surface. Because F_A was unknown, Knohl and Buchmann (2005) modeled it as a saturating function of PAR, which introduced some circularity in their analysis. Instead, we use an entirely empirical function of leaf area index (LAI), photosynthetically active radiation (PAR), the leaf-air water vapor difference (LVD), and the clear sky index χ (i.e. the ratio of observed PAR to the PAR that would have been observed for the same solar zenith angle under clear skies):

$$g_s = \mathrm{LAI}(b_0 e^{b_1 \mathrm{LVD}} e^{b_2 \chi})\mathrm{PAR} \tag{B11}$$

where b_0, b_1, and b_2 are fitted parameters. Transpiration predicted by this function was able to closely reproduce ($r^2 = 0.94$) the measured water flux in manually selected evaporation-free periods throughout the entire growing season using a single set of fitted parameters b_0, b_1, b_2. The r^2 was not appreciably improved by using a curvilinear response to PAR (a Michaelis–Menten function converged to linearity in the fitting), nor by adding dependencies on T_L or soil water content (the fitted scaling factors converged to constants), nor by adding an offset representing stomatal conductance in the dark (the offset converged to $5 \times 10^{-3}\,\mathrm{mol\,m^{-2}\,s^{-1}}$). The observed linear response of g_s to PAR contradicts the common assumption of a saturating response but agrees with some recent sap flux measurements (Schäfer, 2011).

A comparison of our g_s function to EC-derived g_s during a week including rain is shown in Fig. B1. Evaporation following the rain events on 7/18 contaminated Eq. (B9) and caused its EC-derived g_s to surge above g_s from Eq. (B11) (which was fitted to evaporation-free periods only) for about a day in this example, which is from July, when soils were driest. In May, September, and October, when near-surface soil moisture was 40% higher, substantial evaporation sometimes persisted for two or three days following rain. The fact that a single set of fit parameters could reproduce the entire season, including both moist and dry soil periods, suggests that g_s was not significantly affected by soil water in 2011 and that the increased water flux generally observed in the day or two following rain was due to increased evaporation rather than transpiration. Thus use of Eq. (B11) to extrapolate g_s into periods with non-negligible evaporation appears justified. Doing so increased the number of NEE measurements we could safely partition from 337 to 1042. We did not extrapolate to periods with higher (>31 °C) or lower (<18 °C) temperatures or with lower volumetric soil water contents (<19%) than were represented in the evaporation-free periods used to fit Eq. (B11). The mean difference between GEP with and without use of the fitted g_s function in evaporation-free periods over the whole growing season was $-0.06\,\mu\mathrm{mol\,m^{-2}\,s^{-1}}$, which was a proportional difference of −0.3%. The root-mean-square difference was $2.5\,\mu\mathrm{mol\,m^{-2}\,s^{-1}}$, which was 14% of the corresponding mean GEP and is attributable mostly to point-to-point meteorological noise in the g_s from Eq. (B9), as evident in Fig. B1.

We add a few technical notes. First, rather than fitting a function to EC-derived g_s directly, we used Eq. (B9) to convert g_s into transpiration, and fit that to measured E. The idea was to do the fitting in terms of the measured variable so that the measurement noise would be normally distributed and not bias the fit. Second, we selected evaporation-free periods in which to fit our function manually rather than by algorithm because we did not expect the soil hydrology to be sufficiently described by any simple function of our measured variables (e.g. time, net radiation, soil moisture at 15 cm). We began by selecting periods several days after precipitation and excluding most mornings, when canopy dew evaporation was plausible. It was clear from an initial fit of our empirical function that g_s responded consistently to PAR throughout much of this provisional evaporation-free period; the presence or absence of dew evaporation became fairly obvious on many mornings, as did the presence or absence of soil or surface water evaporation on many days. We cropped or expanded our evaporation-free periods accordingly for the final version of the fit, allowing us to include more morning data in particular. Third, though the shape of the response of g_s to PAR, LVD, and χ did not change with wind direction, the magnitude of the response did, consistent with a directional variation in LAI. So, LAI for our calculations (including Eq. (B11)) was inferred for each wind direction as follows: (i) the fitting of Eq. (B11) was initially restricted to the relatively homogeneous sector from 210 to 240° (containing 114 points), (ii) the ratio of g_s from Eq. (B9) to fitted g_s from Eq. (B11) was calculated for all evaporation-free data (376 points), (iii) the natural logarithm of that ratio was smoothed *versus* wind direction using a Loess filter, and (iv) the exponential of the result was multiplied by the site-average LAI to obtain LAI as a smoothly varying function of wind direction (the 376 available points were enough to resolve directional variation with a resolution of around 15° in the data-rich sectors to the west of the tower). The Loess smoothing was done on the logarithm of the ratio so that the result would be a geometric mean (rather than an arithmetic mean), as is appropriate when averaging ratios. The g_s calculation was then repeated using the new direction-dependent LAI as input; one such iteration of the calculation was enough to obtain sufficient convergence in LAI and

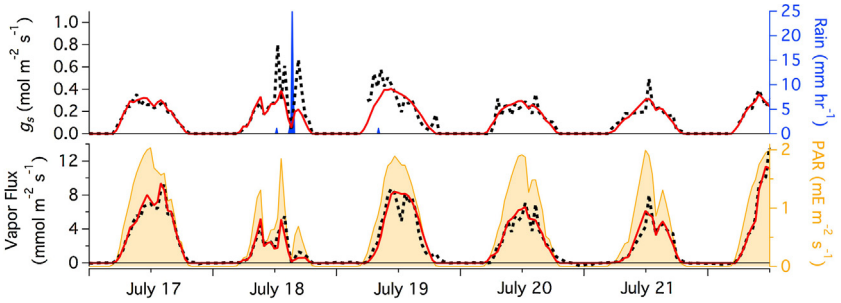

Fig. B1. Time series of stomatal conductance (top panel) and of the water vapor flux (bottom panel) as calculated by eddy covariance (dotted black lines) and by the fitted function described in the text (solid red lines). Also shown are precipitation (blue filled spikes) and PAR (filled yellow). (For interpretation of the references to color in this figure legend, the reader is referred to the web version of this article.)

g_s. The direction-dependent LAI was also used as input to the rest of the IFP calculations.

B.5. Mesophyll resistance

Recent studies have increasingly emphasized the importance of the mesophyll resistance in regulating leaf and canopy scale photosynthesis (Gu and Sun, 2014). The gas-phase equivalent canopy-scale mesophyll resistance $x_m = x_{wp} + x_{ch}$ is considered to vary with LAI and leaf temperature. We convert it to units of s m^{-1} from the mesophyll conductance reported in flux units (g_m^*, in mol m^{-2} s^{-1} rather than m s^{-1}) as:

$$x_m = \frac{1}{g_m^*}\frac{P_a}{RT_L} \tag{B12}$$

where $R = 8.3145$ J mol^{-1} K^{-1} is again the molar gas constant (not an isotope ratio), and where

$$g_m^* = \mathrm{LAI} \cdot \left(0.188 \cdot \exp\left[-0.5\left(\frac{\ln((T_L - 273.15)/28.8)}{0.610}\right)^2\right]\right) \tag{B13}$$

between 10 °C and 35 °C, with T_L in Kelvin (Warren and Dreyer, 2006). The reported uncertainty in Eq. (B13) at the reference temperature of 25 °C is ±0.034 mol m^{-2} s^{-1}, or about ±20% (Warren and Dreyer, 2006). Though Eq. (B13) was obtained for *Quercus canariensis* rather than *Quercus rubra* (both deciduous oaks), it gives $g_m^g = 0.183$ at 25 °C (LAI = 1), in good agreement with the value $g_m^g = 0.175 \pm 0.016$ mol m^{-2} s^{-1} reported for *Quercus rubra* at 25 °C (Manter and Kerrigan, 2004).

A number of studies have reported that mesophyll conductance varies substantially and rapidly in response to environmental conditions, and is tightly correlated with stomatal conductance (see Flexas et al., 2008); however, Tholen et al. (2012) recently pointed out that because photorespiration and foliar daytime 'dark' respiration inject CO_2 into the cytosol (partway through the mesophyll diffusive pathway), the mesophyll conductance measured in those studies is not the true conductance but rather an *apparent* one. Tholen et al. (2012) moreover showed that this apparent conductance will covary with stomatal conductance even when the true mesophyll conductance is constant. Thus it is unclear how the mesophyll resistance varies on short timescales and there is little basis for modeling that variation. For the same reason, the dependence on temperature in Eq. (B13) may be underestimated by 12% or more (Tholen et al., 2012); however, the results of IFP are not sensitive to whether Eq. (B13) or a fixed mesophyll conductance is used.

We divide the total mesophyll resistance x_m into x_{wp} and x_{ch} according to ^{18}O measurements in oak (*Quercus robur*, not *Quercus rubra*) by Gillon and Yakir (2000), who found $g_{ch}/g_{wp} = 3.2$, i.e. $x_{wp} = 0.76x_m$ and $x_{ch} = 0.24x_m$.

B.6. Photocompensation point

The photocompensation point, used in the calculation of the photorespiration flux (Eq. (8)), depends on temperature and O_2 concentration. We know of no temperature-dependent measurements in red oak or red maple, but measurements in *Q. canariensis* (Warren and Dreyer, 2006) agreed well with a function (Brooks and Farquhar, 1985) describing *Spinacia oleracea* (spinach) leaves between 15 and 30 °C at ambient (21%) O_2:

$$\Gamma_*' = 42.7 + 1.68(T_L - 298.15) + 0.0012(T_L - 298.15)^2 \tag{B14}$$

where T_L is in K and Γ_*' is in μmol mol^{-1}. Using spinach data (Jordan and Ogren, 1984), a second, similar equation was derived (Brooks and Farquhar, 1985), putting the photocompensation point about 5% higher than does Eq. (B14) except under rare cold conditions ($T_L < 15$ °C), when the discrepancy is greater.

B.7. Kinetic fractionation by CO_2 fixation

We turn now to the fractionations, beginning with $\varepsilon_f = \alpha_f - 1$, the fractionation by fixation of CO_2 with respect to dissolved CO_2 in the chloroplast. Most CO_2 in C_3 plants is fixed by ribulose 1,5-bisphosphate carboxylase-oxygenase (Rubisco), but some is fixed by phosphoenolpyruvate (PEP) carboxylase (Farquhar and Richards, 1984; Lloyd and Farquhar, 1994). Letting β denote the molar fraction of fixed carbon that is fixed by PEP carboxylase, we can write

$$\alpha_f = \frac{\alpha_{Ru}\alpha_{\mathrm{PEP}}^*}{\beta\alpha_{Ru} + (1-\beta)\alpha_{\mathrm{PEP}}^*} \tag{B15}$$

where α_{Ru} is the fractionation factor for Rubisco carboxylation and α_{PEP}^* is the fractionation factor for PEP carboxylation, both with respect to dissolved CO_2 in the chloroplast. Measurements of β have put it between 0 and 0.15 (Douthe et al., 2012; Lloyd and Farquhar, 1994), with variation between species—e.g. 0.02 for wheat and 0.04 for radish (Caemmerer and Evans, 1991)—and no measurements in oak of which we are aware. We somewhat arbitrarily use $\beta = 0.05$.

The fractionation for Rubisco carboxylation, $\varepsilon_{Ru} = \alpha_{Ru} - 1$, is commonly taken to be constant at 29‰ following Roeske and O'Leary (1984), and that is the value we use here. However, there is in fact very little data on how ε_{Ru} might vary with species or environmental conditions at the precision level desired for the present analysis (~1‰). As summarized in McNevin et al. (2007), most measurements of ε_{Ru} for C_3 plants have used Rubisco from *Spinacia oleracea* (spinach) *in vitro*, for which the reported values range from 26.4 ± 0.6‰ (the value at pH 9.0 in Roeske and O'Leary, 1984) to 30.3 ± 0.8‰ (Guy et al., 1993), with some suggestion that pH

influences the value but conflicting indications as to the direction of that influence. Most early measurements were called into question by Roeske and O'Leary (1984) on account of problems with the method used, known as the combustion method. One early study using the combustion method (Estep et al., 1978) reported a very strong influence (~10‰) of the metal cofactor used for enzyme activation on ε_{Ru}, an issue which appears not to have been explicitly investigated since, using improved methods. The only *in vitro* measurements for C_3 species other than spinach are McNevin et al. (2007)'s measurement for tobacco (27.4 ± 0.9‰), a measurement for cotton (27.1 ± 3.5‰) (Wong et al., 1979), and a measurement for soybean (28.3 ± 1.5‰) (Christeller et al., 1976), the latter two of which used the combustion method. Christeller et al. (1976) is also the only study to have examined the temperature-dependence of ε_{Ru} in C_3 plants, which was a rather large +0.22‰/°C between 15 °C and 35 °C, though Christeller et al. (1976) did not consider this trend significant and the results might be questionable in any case due to use of the combustion method. Christeller et al. (1976) did not report any uncertainties, and their coefficient was reported as −0.22‰/°C because they considered the difference between source and product $\delta^{13}C$ rather than the actual fractionation defined by Eq. (A4). *In vivo* measurements of the combined fractionation due to Rubisco and PEP carboxylase by von Caemmerer and Evans (1991) have suggested that $\varepsilon_{Ru} > 31$‰ for wheat, and that ε_{Ru} differs by at least 4‰ between wheat and radish, although no uncertainties in these values were reported and they should be somewhat in error because they did not take into account the fact that consumption of CO_2 by photosynthesis and release of CO_2 by foliar respiration are not collocated (Tholen et al., 2012).

The fractionation for PEP carboxylation relative to dissolved CO_2 can be broken down further if we assume that carbonic anhydrase is plentiful enough that dissolved CO_2 and bicarbonate are always in equilibrium in the chloroplast. In that case, we can write

$$\alpha^*_{\mathrm{PEP}} = \alpha_{hyd}\alpha_{\mathrm{PEP}} \tag{B16}$$

where α_{hyd} is the equilibrium fractionation factor of hydration (i.e. the $^{13}C/^{12}C$ ratio of the dissolved CO_2 divided by that of the bicarbonate) and α_{PEP} is the kinetic fractionation factor of PEP carboxylase with respect to dissolved bicarbonate. The reported range for $\varepsilon_{\mathrm{PEP}}$ is 2.0–2.5‰ (O'Leary, 1981), and as variation within this range does not much affect IFP, we simply use 2.25‰. For the fractionation by CO_2 hydration, which is known to be dependent on temperature, we use the following empirical formula (Mook et al., 1974):

$$\varepsilon_{\mathrm{hyd}} = -\frac{9866 \pm 230}{T_L + (24.12 \pm 0.78)} \text{ ‰} \tag{B17}$$

with T_L in Kelvin.

We found that ε_f was between 26.9 and 27.3‰ throughout the growing season.

B.8. Kinetic fractionations by photorespiration and daytime 'dark' respiration

Kinetic fractionation by photorespiration depends on the parameter ε and on the fractionation by glycine decarboxylase (g) in Eq. (10). The parameter ε, which relates to the fractionations by aldolase and transketolase, is on the order of 1‰ (Tcherkez, 2006) and its precise value is of only minor importance to IFP (we use 1‰). Fractionation by glycine decarboxylase is dominant, and Tcherkez (2006) suggests the value $g = 22$‰. This value corresponds to $f \sim 11$‰, where f is the apparent photorespiratory fractionation relative to the isotopic composition of recent assimilates, i.e. the same f appearing in the much used equation of Farquhar et al. (1982) for the apparent fractionation by net photosynthetic assimilation of atmospheric CO_2. Published measurements of f have been scattered about 10‰, as discussed in Tcherkez (2006), and $g = 18$‰ seems plausible as well.

The fractionation by daytime 'dark' respiration ε_{DR} (defined relative to a substrate with the same isotopic composition as recent net photosynthetic assimilates) has been theoretically predicted at 5.5‰ (Tcherkez et al., 2004) and estimated from gas exchange measurements at 5 ± 1‰ (Tcherkez et al., 2010). We use $\varepsilon_{DR} = 5$‰, i.e. $\alpha_{DR} = 1.005$ in Eq. (13).

B.9. Equilibrium fractionation by dissolution

The equilibrium fractionation by dissolution of CO_2 in water is also dependent on (leaf) temperature, according to another empirical function (Mook et al., 1974):

$$\varepsilon_d = -\frac{373 \pm 70}{T_L + (0.19 \pm 0.23)} \text{ ‰} \tag{B18}$$

with T_L in Kelvin once again. This formula gives $\varepsilon_d = 1.04‰ \pm 0.04$‰ at 30 °C, in good agreement with the value $\varepsilon_d = 1.1 \pm 0.1$‰ measured by O'Leary (1984).

B.10. Kinetic fractionations by diffusion

The kinetic fractionations by diffusion through the leaf boundary layer, the stomata, and the mesophyll are: $\varepsilon_b = 2.9$‰ (Farquhar et al., 1989), $\varepsilon_s = 4.4$‰ (Farquhar et al., 1989), and $\varepsilon_{wp} = \varepsilon_{ch} = \varepsilon_m = 0.7$‰ (O'Leary, 1984). Here we are assuming that the fractionation for diffusion through the cell wall and plasmalemma (ε_{wp}), as well as that for diffusion through the chloroplast envelope and stroma (ε_{ch}), is simply the fractionation for diffusion of CO_2 through water (0.7‰).

Appendix C. Relation to previous formulations

Aside from a few minor errors, all isoflux-based IFP formulations (Billmark and Griffis, 2009; Bowling et al., 2001; Fassbinder et al., 2012; Knohl and Buchmann, 2005; Lai et al., 2003; Ogée et al., 2003; Zhang et al., 2006; Zobitz et al., 2008) can be obtained from that presented here under various simplifying approximations. The following three approximations were made by all previous IFP studies. First, photorespiration and foliar daytime 'dark' respiration were neglected by assuming $R_P = R_{PR} = R_{DR}$ or, equivalently, $F_{PR} = F_{DR} = 0$ ($F_{PR} = 0 \Leftrightarrow \Gamma'_* = 0$), in which case F_P becomes F_A, and our decomposition $r_m = r_{wp} + r_{ch}$ becomes superfluous. Second, constant values were used (rather than temperature-dependent functions) for the fractionations by dissolution (ε_d) and carboxylation (ε_f), which are sometimes (Bowling et al., 2001; Lai et al., 2003; Zhang et al., 2006) bundled along with the fractionation by mesophyll transport in the single constant parameter b, as in Eq. (4). Finally, photosynthetic fractionation was approximated by Eq. (5), $\varepsilon_A \approx \delta_a - \delta_A$, which introduces non-trivial error, as discussed in Appendix A.

In other approximations, the previous formulations differ from each other. First, all but one formulation (Fassbinder et al., 2012) used an inverted Penman–Monteith (PM) equation (Monteith, 1965) to determine the stomatal resistance, rather than the Fick's law formulation used here (Eqs. (B8)–(B10)). The PM equation was derived to predict evaporation in the absence of sensible heat flux measurements; it too is based on Fick's Law but it uses energy balance and some approximations to eliminate the sensible heat flux as a variable. When sensible heat flux is measured (as at every eddy flux site), it is more accurate and straightforward to use Eqs. (B8)–(B10). Second, all but one formulation (Fassbinder et al., 2012), which was in a chamber study not involving turbulent eddies, calculated the turbulent eddy transport resistance from the momentum analog of Eq. (B1), which requires the poor assumption that the wind speed falls to zero in the canopy airspace, outside the leaf boundary layer. Third, all but two formulations (Fassbinder

et al., 2012; Zobitz et al., 2008) considered the isotopic compositions of the within-canopy and above-canopy air to be the same ($\delta_n = \delta_a$), which is inconsistent with ecosystem source/sink isotopic fractionation. Fourth, only one formulation (Zhang et al., 2006), which was intended for C_4 plants, explicitly considered PEP carboxylase. Fifth, one formulation (Fassbinder et al., 2012) took the net apparent fractionation by diffusion from the canopy air to the chloroplast to be 4.4‰, which is the value strictly appropriate only to the stomatal portion of the pathway. Sixth, some formulations (Bowling et al., 2001; Lai et al., 2003; Zhang et al., 2006) neglected the boundary layer and mesophyll resistances ($r_b = r_m = 0$), while one (Fassbinder et al., 2012) included the mesophyll but not the boundary layer, and the rest (Billmark and Griffis, 2009; Knohl and Buchmann, 2005; Ogée et al., 2003; Zobitz et al., 2008) included both but calculated the boundary layer resistance as a function of a constant Stanton number B, which is an error discussed in Appendix B2.

Finally, it should be noted that none of the previous formulations considered hypostomatous leaves (i.e. leaves with stomates on only the leaf underside, such as those of red oak and red maple, which dominate the canopy of Harvard Forest and many other forests), which require $N = 2$ in Eqs. (B6)–(B7).

References

Amthor, J.S., Goulden, M.L., Munger, J.W., Wofsy, S.C., 1994. Testing a mechanistic model of forest-canopy mass and energy exchange using eddy correlation: carbon dioxide and ozone uptake by a mixed oak-maple stand. Aust. J. Plant. Physiol. 21, 623–651.

Atkin, O.K., Evans, J.R., Siebke, K., 1998. Relationship between the inhibition of leaf respiration by light and enhancement of leaf dark respiration following light treatment. Aust. J. Plant Physiol. 25, 437–443, http://dx.doi.org/10.1071/PP97159.

Baldocchi, D.D., 2008. "Breathing" of the terrestrial biosphere: lessons learned from a global network of carbon dioxide flux measurement systems. Aust. J. Bot. 56, 1–26, http://dx.doi.org/10.1071/BT07151.

Baldocchi, D.D., Bowling, D.R., 2003. Modelling the discrimination of $^{13}CO_2$ above and within a temperate broad-leaved forest canopy on hourly to seasonal time scales. Plant Cell Environ. 26, 231–244.

Bauwe, H., Hagemann, M., Fernie, A.R., 2010. Photorespiration: players, partners and origin. Trends Plant Sci. 15, 330–336, http://dx.doi.org/10.1016/j.tplants.2010.03.006.

Betson, N.R., Göttlicher, S.G., Hall, M., Wallin, G., Richter, A., Högberg, P., 2007. No diurnal variation in rate or carbon isotope composition of soil respiration in a boreal forest. Tree Physiol. 27, 749–756.

Billesbach, D.P., Berry, J.A., Seibt, U., Maseyk, K., Torn, M.S., Fischer, M.L., Abu-Naser, M., Campbell, J.E., 2014. Growing season eddy covariance measurements of carbonyl sulfide and CO_2 fluxes: COS and CO_2 relationships in Southern Great Plains winter wheat. Agric. For. Meteorol. 184, 48–55, http://dx.doi.org/10.1016/j.agrformet.2013.06.007.

Billmark, K.A., Griffis, T.J., 2009. Influence of phenology and land management on biosphere–atmosphere isotopic CO_2 exchange. In: Phenology of Ecosystem Processes. Springer, New York, NY, pp. 143–166, http://dx.doi.org/10.1007/978-1-4419-0026-5_6.

Bowling, D.R., Ballantyne, A.P., Miller, J.B., Burns, S.P., Conway, T.J., Menzer, O., Stephens, B.B., Vaughn, B.H., 2014. Ecological processes dominate the ^{13}C land disequilibrium in a Rocky Mountain subalpine forest. Glob. Biogeochem. Cycles 28, 352–370, http://dx.doi.org/10.1002/2013GB004686.

Bowling, D.R., Egan, J.E., Hall, S.J., Risk, D.A., 2015. Environmental forcing does not induce diel or synoptic variation in carbon isotope content of forest soil respiration. Biogeosci. Discuss. 12, 6361–6404, http://dx.doi.org/10.5194/bgd-12-6361-2015.

Bowling, D.R., Tans, P.P., Monson, R.K., 2001. Partitioning net ecosystem carbon exchange with isotopic fluxes of CO_2. Glob. Change Biol. 7, 127–145.

Breda, N.J.J., 2003. Ground-based measurements of leaf area index: a review of methods, instruments and current controversies. J. Exp. Bot. 54, 2403–2417, http://dx.doi.org/10.1093/jxb/erg263.

Brooks, A., Farquhar, G.D., 1985. Effect of temperature on the CO_2/O_2 specificity of ribulose-1,5-bisphosphate carboxylase/oxygenase and the rate of respiration in the light. Planta 165, 397–406.

Caemmerer, von S., Evans, J.R., 1991. Determination of the average partial pressure of CO_2 in chloroplasts from leaves of several C3 plants. Aust. J. Plant Physiol. 18, 287–305.

Christeller, J.T., Laing, W.A., Troughton, J.H., 1976. Isotope discrimination by ribulose 1,5-diphosphate carboxylase. Plant Physiol. 57, 580–582.

Collatz, G.J., Ball, J.T., Grivet, C., Berry, J.A., 1991. Physiological and environmental regulation of stomatal conductance, photosynthesis and transpiration: a model that includes a laminar boundary layer. Agric. For. Meteorol. 54, 107–136.

Coplen, T.B., 2011. Guidelines and recommended terms for expression of stable-isotope-ratio and gas-ratio measurement results. Rapid Commun. Mass Spectrom. 25, 2538–2560.

De Pury, D.G.G., Farquhar, G.D., 1997. Simple scaling of photosynthesis from leaves to canopies without the errors of big-leaf models. Plant Cell Environ. 20, 537–557, http://dx.doi.org/10.1111/j.1365-3040.1997.00094.x.

Douthe, C., Dreyer, E., Brendel, O., Warren, C.R., 2012. Is mesophyll conductance to CO_2 in leaves of three Eucalyptus species sensitive to short-term changes of irradiance under ambient as well as low O_2? Funct. Plant Biol. 39, 435–448, http://dx.doi.org/10.1071/FP11190.

Estep, M.F., Tabita, F.R., Parker, P.L., Van Baalen, C., 1978. Carbon isotope fractionation by ribulose-1,5-bisophosphate carboxylase from various organisms. Plant Physiol. 61, 680–687.

Evans, J.R., Caemmerer, von S., 1996. Carbon dioxide diffusion inside leaves. Plant Physiol. 110, 339–346.

Farquhar, G., O'Leary, M.H., Berry, J.A., 1982. On the relationship between carbon isotope discrimination and the intercellular carbon dioxide concentration in leaves. Aust. J. Plant Physiol. 9, 121–137.

Farquhar, G.D., Ehleringer, J.R., Hubick, K.T., 1989. Carbon isotope discrimination and photosynthesis. Annu. Rev. Plant Physiol. Plant Mol. Biol. 40, 503–537.

Farquhar, G.D., Richards, R.A., 1984. Isotopic composition of plant carbon correlates with water-use efficiency of wheat genotypes. Aust. J. Plant Physiol. 11, 539–552, http://dx.doi.org/10.1071/PP9840539.

Fassbinder, J.J., Griffis, T.J., Baker, J.M., 2012. Evaluation of carbon isotope flux partitioning theory under simplified and controlled environmental conditions. Agric. For. Meteorol. 153, 154–164.

Flexas, J., Ribas Carbó, M., Diaz-Espejo, A., Galmés, J., Medrano, H., 2008. Mesophyll conductance to CO_2: current knowledge and future prospects. Plant 31, 602–621.

Gatz, D.F., Smith, L., 1995. The standard error of a weighted mean concentration—I. Bootstrapping vs other methods. Atmos. Environ. 29, 1185–1193, http://dx.doi.org/10.1016/1352-2310(94)00210-C.

Ghashghaie, J., Badeck, F.-W., Lanigan, G., Nogués, S., Tcherkez, G., Deléens, E., Cornic, G., Griffiths, H.G., 2003. Carbon isotope fractionation during dark respiration and photorespiration in C3 plants. Phytochem. Rev. 2, 145–161.

Gillon, J.S., Yakir, D., 2000. Internal conductance to CO_2 diffusion and C18OO discrimination in C3 leaves. Plant Physiol. 123, 201–213.

Goulden, M.L., Munger, J.W., Fan, S.-M., Daube, B.C., Wofsy, S.C., 1996. Measurements of carbon sequestration by long-term eddy covariance: methods and a critical evaluation of accuracy. Glob. Change Biol. 2, 169–182.

Griffis, T.J., Baker, J.M., Sargent, S.D., Tanner, B.D., Zhang, J., 2004. Measuring field-scale isotopic CO_2 fluxes with tunable diode laser absorption spectroscopy and micrometeorological techniques. Agric. For. Meteorol. 124, 15–29.

Gu, L., Sun, Y., 2014. Artefactual responses of mesophyll conductance to CO_2 and irradiance estimated with the variable J and online isotope discrimination methods. Plant Cell Environ. 37, 1231–1249, http://dx.doi.org/10.1111/pce.12232.

Guy, R.D., Fogel, M.L., Berry, J.A., 1993. Photosynthetic fractionation of the stable isotopes of oxygen and carbon. Plant Physiol. 101, 37–47.

Heskel, M.A., Atkin, O.K., Turnbull, M.H., Griffin, K.L., 2013. Bringing the Kok effect to light: A review on the integration of daytime respiration and net ecosystem exchange. Ecosphere 4 (98), 1–14.

Hicks, B.B., Baldocchi, D.D., Meyers, T.P., Hosker Jr., R.P., Matt, D.R., 1987. A preliminary multiple resistance routine for deriving dry deposition velocities from measured quantities. Water Air Soil Pollut. 36, 311–330.

Hurry, V., Igamberdiev, A.U., Keerberg, O., Pärnik, T., Atkin, O.K., Zaragoza-Castells, J., Gardeström, P., 2005. Respiration in photosynthetic cells: gas exchange components, interactions with photorespiration and the operation of mitochondria in the light. In: Lambers, H., Ribas-Carbo, M. (Eds.), Plant Respiration. Springer-Verlag, Berlin/Heidelberg, pp. 43–61, http://dx.doi.org/10.1007/1-4020-3589-6_4.

Igamberdiev, A.U., Mikkelsen, T.N., Ambus, P., Bauwe, H., Lea, P.J., Gardeström, P., 2004. Photorespiration contributes to stomatal regulation and carbon isotope fractionation: a study with barley, potato and *Arabidopsis* plants deficient in glycine decarboxylase. Photosynth. Res. 81, 131–152.

Joiner, J., Guanter, L., Lindstrot, R., Voigt, M., Vasilkov, A.P., Middleton, E.M., Huemmrich, K.F., Yoshida, Y., Frankenberg, C., 2013. Global monitoring of terrestrial chlorophyll fluorescence from moderate-spectral-resolution near-infrared satellite measurements: methodology. Simul. Appl. GOME-2, http://dx.doi.org/10.5194/amt-6-2803-2013.

Jordan, D.B., Ogren, W.L., 1984. The CO_2/O_2 specificity of ribulose 1,5-bisphosphate carboxylase/oxygenase. Planta 161, 308–313, http://dx.doi.org/10.1007/BF00398720.

Klemm, O., Milford, C., Sutton, M.A., Spindler, G., van Putten, E., 2002. A climatology of leaf surface wetness. Theor. Appl. Climatol. 71, 107–117.

Knohl, A., Buchmann, N., 2005. Partitioning the net CO_2 flux of a deciduous forest into respiration and assimilation using stable carbon isotopes. Glob. Biogeochem. Cycles 19, GB4008, http://dx.doi.org/10.1029/2004GB002301.

Kucharik, C.J., Norman, J.M., Gower, S.T., 1998. Measurements of branch area and adjusting leaf area index indirect measurements. Agric. For. Meteorol. 91, 69–88.

Lai, C.-T., Schauer, A.J., Owensby, C., Ham, J.M., Ehleringer, J.R., 2003. Isotopic air sampling in a tallgrass prairie to partition net ecosystem CO2 exchange. J. Geophys. Res. 108, 4566, http://dx.doi.org/10.1029/2002JD003369.

Lamaud, E., Brunet, Y., Labatut, A., Lopez, A., Fontan, J., Druilhet, A., 1994. The Landes experiment: biosphere–atmosphere exchanges of ozone and aerosol particles above a pine forest. J. Geophys. Res. 99, 16–511–16–521.
Lanigan, G.J., Betson, N., Griffiths, H., Seibt, U., 2008. Carbon isotope fractionation during photorespiration and carboxylation in Senecio. Plant Physiol. 148, 2013–2020, http://dx.doi.org/10.1104/pp.108.130153.
Lasslop, G., Reichstein, M., Papale, D., Richardson, A.D., Arneth, A., Barr, A., Stoy, P.C., Wohlfahrt, G., 2010. Separation of net ecosystem exchange into assimilation and respiration using a light response curve approach: critical issues and global evaluation. Glob. Change Biol. 16, 187–208.
Lee, X., Griffis, T.J., Baker, J.M., Billmark, K.A., Kim, K., Welp, L.R., 2009. Canopy-scale kinetic fractionation of atmospheric carbon dioxide and water vapor isotopes. Glob. Biogeochem. Cycles 23, 1–15, http://dx.doi.org/10.1029/2008GB003331.
Lloyd, J., Farquhar, G.D., 1994. ^{13}C discrimination during CO_2 assimilation by the terrestrial biosphere. Oecologia 99, 201–215, http://dx.doi.org/10.1007/BF00627732.
Lloyd, J., Grace, J., Miranda, A.C., Meir, P., Wong, S.C., Miranda, H.S., Wright, I.R., Gash, J.H.C., McIntyre, J., 1995. A simple calibrated model of Amazon rainforest productivity based on leaf biochemical properties. Plant Cell Environ. 18, 1129–1145.
Luyssaert, S., Inglima, I., Jung, M., 2009. Global Forest Ecosystem Structure and Function Data for Carbon Balance Research., http://dx.doi.org/10.3334/ORNLDAAC/949.
Manter, D.K., Kerrigan, J., 2004. A/Ci curve analysis across a range of woody plant species: influence of regression analysis parameters and mesophyll conductance. J. Exp. Bot. 55, 2581–2588, http://dx.doi.org/10.1093/jxb/erh260.
Massman, W.J., 1999. A model study of kBH-1 for vegetated surfaces using "localized near-field" Lagrangian theory. J. Hydrol. 223, 27–43, http://dx.doi.org/10.1016/S0022-1694(99)00104-3.
McNaughton, K.G., Hurk, B., 1995. A "Lagrangian" revision of the resistors in the two-layer model for calculating the energy budget of a plant canopy. Bound.-Layer Meteorol. 74, 261–288.
McNevin, D.B., Badger, M.R., Whitney, S.M., Caemmerer, von S., Tcherkez, G.G.B., Farquhar, G.D., 2007. Differences in carbon isotope discrimination of three variants of D-ribulose-1,5-bisphosphate carboxylase/oxygenase reflect differences in their catalytic mechanisms. J. Biol. Chem. 282, 36068–36076, http://dx.doi.org/10.1074/jbc.M706274200.
Monteith, J., 1965. Evaporation and environment. Symp. Soc. Exp. Biol. 19, 205–234.
Mook, W.G., Bommerson, J.C., Staverman, W.H., 1974. Carbon isotope fractionation between dissolved bicarbonate and gaseous carbon dioxide. Earth Planet. Sci. Lett. 22, 169–176, http://dx.doi.org/10.1016/0012-821X(74)90078-8.
Mott, K.A., O'Leary, M.H., 1984. Stomatal behavior and CO_2 exchange characteristics in amphistomatous leaves. Plant Physiol. 74, 47–51.
Nogués, S., Tcherkez, G., Cornic, G., Ghashghaie, J., 2004. Respiratory carbon metabolism following illumination in intact French bean leaves using $^{13}C/^{12}C$ isotope labeling. Plant Physiol. 136, 3245–3254.
O'Leary, M.H., 1984. Measurement of the isotope fractionation associated with diffusion of carbon dioxide in aqueous solution. J. Phys. Chem. 88, 823–825.
O'Leary, M.H., 1981. Carbon isotope fractionation in plants. Phytochemistry 20, 553–567, http://dx.doi.org/10.1016/0031-9422(81)85134-5.
Ogée, J., Peylin, P., Ciais, P., Bariac, T., Brunet, Y., Berbigier, P., Roche, C., Richard, P., Bardoux, G., Bonnefond, J., 2003. Partitioning net ecosystem carbon exchange into net assimilation and respiration using $^{13}CO_2$ measurements: a cost-effective sampling strategy. Glob. Biogeochem. Cycles 17, 1070.
Owen, P.R., Thomson, W.R., 1963. Heat transfer across rough surfaces. J. Fluid Mech. 15, 321–334, http://dx.doi.org/10.1017/S0022112063000288.
Parkhurst, D.F., Mott, K.A., 1990. Intercellular diffusion limits to CO_2 uptake in leaves. Plant Physiol. 94, 1024–1032.
Pärnik, T., Ivanova, H., Keerberg, O., 2007. Photorespiratory and respiratory decarboxylations in leaves of C3 plants under different CO_2 concentrations and irradiances. Plant Cell Environ. 30, 1535–1544, http://dx.doi.org/10.1111/j.1365-3040.2007.01725.x.
Pärnik, T., Keerberg, O., 2007. Advanced radiogasometric method for the determination of the rates of photorespiratory and respiratory decarboxylations of primary and stored photosynthates under steady-state photosynthesis. Physiol. Plant 129, 34–44.
Raupach, M., Thom, A.S., 1981. Turbulence in and above plant canopies. Annu. Rev. Fluid Mech. 13, 97–129.
Reichstein, M., Falge, E., Baldocchi, D.D., Papale, D., Aubinet, M., Berbigier, P., Bernhofer, C., Buchmann, N., Gilmanov, T., Granier, A., Grünwald, T., Havrankova, K., Ilvesniemi, H., Janous, D., Knohl, A., Laurila, T., Lohila, A., Loustau, D., Matteucci, G., MEYERS, T., Miglietta, F., Ourcival, J.-M., Pumpanen, J., Rambal, S., Rotenberg, E., Sanz, M., Tenhunen, J., Seufert, G., Vaccari, F., Vesala, T., Yakir, D., Valentini, R., 2005. On the separation of net ecosystem exchange into assimilation and ecosystem respiration: review and improved algorithm. Glob. Change Biol. 11, 1424–1439, http://dx.doi.org/10.1111/j.1365-2486.2005.001002.x.
Roeske, C.A., O'Leary, M.H., 1984. Carbon isotope effects on enzyme-catalyzed carboxylation of ribulose bisphosphate. Biochemistry 23, 6275–6284, http://dx.doi.org/10.1021/bi00320a058.
Scanlon, T.M., Kustas, W.P., 2010. Partitioning carbon dioxide and water vapor fluxes using correlation analysis. Agric. For. Meteorol. 150, 89–99, http://dx.doi.org/10.1016/j.agrformet.2009.09.005.
Schäfer, K.V.R., 2011. Canopy stomatal conductance following drought, disturbance, and death in an upland oak/pine forest of the New Jersey Pine Barrens, USA. Front. Plant Sci. 2, 1–7, http://dx.doi.org/10.3389/fpls.2011.00015.
Schuepp, P., 1993. Leaf boundary layers. N. Phytol. 125, 477–507.
Sharkey, T.D., 1988. Estimating the rate of photorespiration in leaves. Physiol. Plant 73, 147–152, http://dx.doi.org/10.1111/j.1399-3054.1988.tb09205.x.
Siegenthaler, U., Munnich, K., 1981. $^{13}C/^{12}C$ fractionation during CO_2 transfer from air to sea. In: Bolin, B. (Ed.), Carbon Cycle Modelling. John Wiley, New York, pp. 249–257.
Stoy, P.C., Katul, G.G., Siqueira, M.B.S., Juang, J.-Y., Novick, K.A., Uebelherr, J.M., Oren, R., 2006. An evaluation of models for partitioning eddy covariance-measured net ecosystem exchange into photosynthesis and respiration. Agric. For. Meteorol. 141, 2–18, http://dx.doi.org/10.1016/j.agrformet.2006.09.001.
Tans, P., Berry, J., Keeling, R., 1993. Oceanic $^{13}C/^{12}C$ observations: a new window on ocean CO_2 uptake. Glob. Biogeochem. Cycles.
Tcherkez, G., 2006. Viewpoint: how large is the carbon isotope fractionation of the photorespiratory enzyme glycine decarboxylase? Funct. Plant Biol. 33, 911, http://dx.doi.org/10.1071/FP06098.
Tcherkez, G., Farquhar, G., Badeck, F., Ghashghaie, J., 2004. Theoretical considerations about carbon isotope distribution in glucose of C3 plants. Funct. Plant Biol. 31, 857, http://dx.doi.org/10.1071/FP04053.
Tcherkez, G., Schäufele, R., Nogués, S., Piel, C., Boom, A., Lanigan, G., Barbaroux, C., Mata, C., Elhani, S., Hemming, D., Maguas, C., Yakir, D., Badeck, F.W., Griffiths, H., Schnyder, H., Ghashghaie, J., 2010. On the $^{13}C/^{12}C$ isotopic signal of day and night respiration at the mesocosm level. Plant Cell Environ. 33, 900–913, http://dx.doi.org/10.1111/j.1365-3040.2010.02115.x.
Tholen, D., Ethier, G., Genty, B., Pepin, S., Zhu, X.-G., 2012. Variable mesophyll conductance revisited: theoretical background and experimental implications. Plant Cell Environ. 35, 2087–2103, http://dx.doi.org/10.1111/j.1365-3040.2012.02538.x.
Urbanski, S., Barford, C., Wofsy, S., Kucharik, C., Pyle, E., Budney, J., McKain, K., Fitzjarrald, D., Czikowsky, M., Munger, J.W., 2007. Factors controlling CO_2 exchange on timescales from hourly to decadal at Harvard Forest. J. Geophys. Res. 112, G02020, http://dx.doi.org/10.1029/2006JG000293.
Warren, C.R., Dreyer, E., 2006. Temperature response of photosynthesis and internal conductance to CO2: results from two independent approaches. Journal of Experimental Botany 57 (12), 3057–3067, http://dx.doi.org/10.1093/jxb/erl067.
Wehr, R., Munger, J.W., Nelson, D.D., McManus, J.B., Zahniser, M.S., Wofsy, S.C., Saleska, S.R., 2013. Long-term eddy covariance measurements of the isotopic composition of the ecosystem–atmosphere exchange of CO_2 in a temperate forest. Agric. For. Meteorol. 181, 69–84, http://dx.doi.org/10.1016/j.agrformet.2013.07.002.
Wofsy, S.C., Goulden, M.L., Munger, J.W., Fan, S.-M., Bakwin, P., Daube, B.C., Bassow, S., Bazzaz, F., 1993. Net exchange of CO_2 in a mid-latitude forest. Science 260, 1314–1317.
Wohlfahrt, G., Brilli, F., Hörtnagl, L., Xu, X., Bingemer, H., Hansel, A., Loreto, F., 2011. Carbonyl sulfide (COS) as a tracer for canopy photosynthesis, transpiration and stomatal conductance: potential and limitations. Plant Cell Environ. 35, 657–667, http://dx.doi.org/10.1111/j.1365-3040.2011.02451.x.
Wong, W.W., Benedict, C.R., Kohel, R.J., 1979. Enzymic fractionation of the stable carbon isotopes of carbon dioxide by ribulose-1,5-bisphosphate carboxylase. Plant Physiol. 63, 852–856.
World Meteorological Organization, 2008. Guide to Meteorological Instruments and Methods of Observation (No. WMO-No. 8). World Meteorological Organization, Geneva.
Xu, C.-Y., Griffin, K.L., 2008. Scaling foliar respiration to the stand level throughout the growing season in a *Quercus rubra* forest. Tree Physiol. 28, 637–646.
Yakir, D., Wang, X., 1996. Fluxes of CO_2 and water between terrestrial vegetation and the atmosphere estimated from isotope measurements. Nature 380, 515–517.
Zhang, J., Griffis, T.J., Baker, J.M., 2006. Using continuous stable isotope measurements to partition net ecosystem CO_2 exchange. Plant Cell Environ. 29, 483–496, http://dx.doi.org/10.1111/j.1365-3040.2005.01425.x.
Zobitz, J.M., Burns, S.P., Reichstein, M., Bowling, D.R., 2008. Partitioning net ecosystem carbon exchange and the carbon isotopic disequilibrium in a subalpine forest. Glob. Change Biol. 14, 1785–1800, http://dx.doi.org/10.1111/j.1365-2486.2008.01609.x.